Paleoenvironmental signature of the Selandian-Thanetian Transition Event (STTE) and Early Late Paleocene Event (ELPE) in the Contessa Road section (western Neo-Tethys)

Rodolfo Coccioni, Fabrizio Frontalini, Rita Catanzariti, Luigi Jovane, Daniel Rodelli, Ianco M M Rodrigues, Jairo F Savian, Martino Giorgioni, Bruno Galbrun

Palaeogeography, Palaeoclimatology, Palaeoecology
Volume 523, 2019, Pages 62-77

Paleoenvironmental signature of the Selandian-Thanetian Transition Event (STTE) and Early Late Paleocene Event (ELPE) in the Contessa Road section (western Neo-Tethys)

RodolfoCoccioni[a], Fabrizio Frontalini[a], Rita Catanzariti[b], Luigi Jovane[c], Daniel Rodelli[c], Ianco M.M. Rodrigues[c], Jairo F. Savian[d], Martino Giorgioni[e], Bruno Galbrun[f]

a Dipartimento di Scienze Pure e Applicate, Università degli Studi di Urbino "Carlo Bo", Campus Scientifico, Località Crocicchia, 61029 Urbino, Italy
b Istituto di Geoscienze e Georisorse, CNR, 56124 Pisa, Italy
c Departamento de Oceanografia Física, Instituto Oceanográfico, Universidade de São Paulo, Praça do Oceanográfico, 191, 05508-120 São Paulo, Brazil
d Departamento de Geologia, Instituto de Geociências, Universidade Federal do Rio Grande do Sul, Av. Bento Gonçalves, 9500, 91501-970 Porto Alegre, Brazil
e Instituto de Geociências da Universidade de Brasília, Campus Universitário Darcy Ribeiro ICC - Ala Central, 70910-900 Brasília, DF, Brazil
f Université Paris VI, CNRS–UMR 7193, ISTeP 'Institut des Sciences de la Terre-Paris', case117, 4, place Jussieu, 75252 Paris Cedex 05, France

Abstract

Sedimentary records of the Early Cenozoic indicate a series of events with climatic and carbon cycle variability known as hyperthermals. A ~350-kyr-long event of environmental disruption during the Paleocene, not described before and here named Selandian–Thanetian Transition Event (STTE), has been recognized and well constrained in the western Tethys Contessa Road section (Gubbio, Italy) through high-resolution biostratigraphic, geochemical, and rock-magnetic data. The STTE exhibits peculiar stressed ecological responses among calcareous nannofossils and foraminifera, which highlight marked environmental perturbation affecting the biosphere. The environmental instability is not confined within the photic zone but extends to the seafloor leading to little more trophic conditions of the sea surface waters with an enhanced, but of short measure, nutrient availability on the seafloor conditions and marked rise of lysocline. Magnetic Susceptibly (MS) is dominantly controlled by the balance between carbonate productivity and detrital supply, as evidenced by the strong correlation between MS and CaCO3 (%) ($r2 = -0.72$). However, we also document two components in the isothermal remanent magnetization (IRM) and first-order reversal curves (FORC) diagrams that prove the occurrence of biogenic magnetite throughout the STTE. Systematic variations in bio-geochemical and magnetic parameters show the relative abundance of carbonate production (or inversely dissolution of carbonate) versus detrital supply during the STTE, which induced higher populations of magnetotactic bacteria through increased terrigenous input and, therefore, increased nutrient supply. Noteworthy, the uppermost part of the STTE includes the equivalent of the suspected hyperthermal, short-lived Early Late Paleocene Event (ELPE). The ELPE event shows an episode of increase in magnetic properties of the sediments, including an increase in magnetofossil concentration, as indicated by IRM components and FORC diagrams. The comparison of biotic and abiotic records throughout the STTE at Contessa Road section with available data across the ELPE from former investigated ocean and land-based sites provides lines of evidence that this latter event might be indeed only the terminal part of a long-lasting environmental change than hitherto supposed.

Keywords : Magnetofossils, Hyperthermal, ELPE, Dissolution, Umbria-Marche Basin

1. Introduction

The lower-middle Paleogene has been perturbed by a series of transient (104 to 105 years) warming events termed hyperthermals that have been associated with changes in the carbon isotope composition of the ocean–climate system (Cramer et al., 2003). The input of carbon is evidenced by prominent negative carbon isotope excursions (CIEs) in carbonate and organic matter (Zachos et al., 2004, Zachos et al., 2005). The presence of distinct clay layers associated with abrupt drops in carbonate content and pronounced peaks in magnetic susceptibility characterize these intervals. These levels have been interpreted as the sedimentary expression of abrupt climatic changes associated with increasing atmospheric pCO2, substantial shoaling of the lysocline and of the calcite compensation depth (CCD), and a general lowering of the carbonate saturation state (Zachos et al., 2005) potentially induced, for some events, like the Paleocene-Eocene Thermal Maximum (PETM) by the dissociation of gas hydrates (Dickens et al., 1995, Dickens et al., 1997). Accelerated hydrologic and invigorated weathering cycles inferred from more marginal settings (Bowen et al., 2004; Pagani et al., 2006; Sluijs et al., 2007) might suggest an enhanced seasonality concomitant with peak of humid phases (Jovane et al., 2010).
The early late Paleocene hyperthermal event (ELPE, Bralower et al., 2002), also known as the mid-Paleocene biotic event (MPBE, Bernaola et al., 2007), is a climatic perturbation occurring in the Late Paleocene, between the Selandian and the Thanetian stages. It has been recognized in several deep-sea cores from the Shatsky Rise (ODP Leg 198, central Pacific), Walvis Ridge (ODP Leg 208, South Atlantic), Maud Rise (ODP Leg 113, Weddell Sea) and Black Nose (ODP Leg 171, North Atlantic) as well as in on–land Spanish (Zumaia, Ibaeta, and Rìo Gor), Italian (Contessa Road) Tunisian (Tejerouine), Moroccan (Ouled Abdoun basin), Egyptian (Naqb El-Rufuf) and Mead Stream (New Zealand) sections, and on terrestrial paleosol record (Cerro Bayo, Argentina) (Bralower et al., 2002; Zachos et al., 2004; Petrizzo, 2005; Bernaola et al., 2007; Westerhold et al., 2011; Coccioni et al., 2012; Karoui-Yaakoub et al., 2014; Kocsis et al., 2014; Littler et al., 2014; Pujalte et al., 2014, Pujalte et al., 2016; Hyland et al., 2015; Hewaidy et al., 2019) (Fig. 1). At Shatsky Rise, this hyperthermal event falling in the lower part of planktonic foraminiferal P4 Zone of Berggren et al. (1995) and coinciding with the evolutionary lowest occurrence (LO) of Heliolithus kleinpellii, which marks the base of calcareous nannofossil Zones NP6 of Martini (1971) and CP5 of Okada and Bukry (1980) corresponds to a prominent peak in magnetic susceptibility, significant changes and turnovers in foraminiferal assemblages, carbonate dissolution, and sea surface warming (Bralower et al., 2002; Petrizzo, 2005; Hancock and Dickens, 2005; Bralower et al., 2006; Littler et al., 2014). Hancock and Dickens (2005) highlighted that the event marks a short extreme within the context of a longer 1–2 My interval of odd conditions. This supports the hypothesis of a prominent change in ocean circulation as also corroborated by the occurrence of clay-rich intervals (Killops et al., 2000; Zachos et al., 2004; Hollis et al., 2005; Bernaola et al., 2007). Agnini et al. (2007) related the consecutive appearances of the genera Heliolithus, Discoasteroides, and Discoaster to environmental perturbations at the onset, during, and after the ELPE transient event, respectively. The onset of the ELPE has been constrained to the uppermost part of Chron C26r and its end to the middle part of Chron C26n (Agnini et al., 2007). The Zumaia section represents the first land-based locality where the MPBE was documented and described in detail (Bernaola et al., 2007). On the basis of micropaleontological analyses, a shift from relatively cooler mesotrophic to warmer oligotrophic conditions, probably induced by an input of isotopically depleted carbon triggering a rapid shoaling of the lysocline, was suggested (Bernaola et al., 2007). The Cerro Bayo section representing the first terrestrial record where the MPBE was identified, the event occurs as a two-stage transient hyperthermal event (MPBE and MPBE-2) related to increasing mean annual temperatures and shifts in precipitation in the regional climate (Hyland et al., 2015). In the Tethys, a series of biotic and environmental changes occurs between the Selandian and the Thanetian, defining the Selandian-Thanetian Transition Event (STTE; Coccioni et al., 2012). However, the relationship between STTE and ELPE is still not well characterized. Here, we document and characterize the significant biotic and abiotic changes across the Selandian–Thanetian transition in the western Tethys Contessa Road section (Gubbio, Italy). By comparing it with coeval deep-sea sites and land-based sections, we also show that the ELPE might be part of a scenario more complex than previously supposed. Furthermore, we integrate paleoclimatic and paleoceanographic proxies with environmental magnetism and identification of magnetofossils. The abundance of biogenic magnetite in marine sediments can be used as a proxy for paleoproductivity, which is mainly controlled by nutrient limitation, organic carbon supply, iron availability, and redox conditions (e.g., Roberts et al., 2011, Roberts et al., 2012, Roberts et al., 2013; Larrasoaña et al., 2012; Chang et al., 2012, Chang et al., 2018; Yamazaki and Ikehara, 2012; Savian et al., 2014, Savian et al., 2016; Liu et al., 2015; Yamazaki and Horiuchi, 2016). This large dataset allows new paleoceanographic and paleoclimatic reconstruction across STTE and ELPE events.

2. Location and stratigraphic setting

The Contessa Road section (lat. 43°22′47″N; long. 13°33′49″E), located near Gubbio (central Italy), is one of the most representative Tethyan successions for the Mesozoic–Cenozoic (e.g., Coccioni et al., 2010, Coccioni et al., 2012, Coccioni et al., 2013). In particular, it represents a continuous and complete record suitable for correlating the early-middle Paleogene biostratigraphy to the geomagnetic polarity history. The Contessa Road section spans from the upper Danian to the middle Ypresian. It consists of well–bedded pink to red, occasionally white, limestones and marly limestones with red marly interbeds at the Selandian–Thanetian transition and from the upper Thanetian to the middle Ypresian (Coccioni et al., 2013, Coccioni et al., 2016). This ~56 m-thick section of pelagic sediments belongs to the "Scaglia"-type facies and is made up of well-stratified coccolith-foraminiferal limestones with subordinated marls deposited at lower middle to lower bathyal depths (1000–1500 m) (Coccioni et al., 2013). The 8-m thick interval spanning from 16 to 24 m above the Cretaceous-Paleogene (K–Pg) boundary is characterized by the occurrence of six marly beds at 17.70–17.75, 18.37–18.47 m, 20.05–20.09 m, 20.15–20.17 m, 20.75–20.95 m and 21.88–21.92 m (Fig. 2). Particular emphasis is given to the 18–22 m studied interval, where Coccioni et al. (2012) inferred significant biotic and abiotic changes. Following Coccioni et al. (2016), the average sedimentation rate for the Paleocene of the Contessa Highway-Contessa Road composite section is ~5 m/Myr, the studied interval would therefore span ~800 kyr.

3. Material and methods

3.1. Sampling

A total of sixty-one bulk rock samples were collected for calcium carbonate, bulk isotopic, magnetostratigraphy, environmental and rock magnetic, and micropaleontological analyses throughout the studied segment (Fig. 2) at an average spacing of ~13 cm, corresponding to ~26 kyr. For low-field mass-specific magnetic susceptibility (χ) and environmental magnetism, four hundred samples were collected at 2 cm intervals corresponding to ~4 kyr (Appendix A, Appendix B). Representative samples were selected along the section for rock magnetic measurements (isothermal remanent magnetization acquisition curves, hysteresis loops, and first-order reversal curves).

3.2. Geochemistry

Analyses of carbonate content were performed at the geochemistry laboratory of the Dipartimento di Scienze Pure e Applicate, Università di Urbino (Italy). The bulk rock samples were reduced to fine powder in an agate mortar. Calcium carbonate content measurements were obtained using a Dietrich–Frühling calcimeter. The method is based on the measurement of CO_2 volume produced by the complete dissolution of pre-weighted samples (300 ± 1 mg each) in 10 vol% HCl. Total carbonate contents (wt% $CaCO_3$) were computed with a precision of 1% using formulae that take into account pressure and temperature of the lab environment, amount of bulk sample used, and the volume of CO_2 developed in the calcimeter. Standards of pure calcium carbonate (i.e., Carrara Marble) were measured every ten samples to ensure proper calibration (Appendix A).
Stable isotope analyses ($\delta^{18}O$ and $\delta^{13}C$) were conducted using an automated continuous-flow carbonate preparation GasBenchII device (Spötl and Vennemann, 2003) and a ThermoElectron Delta Plus XP mass spectrometer in the geochemistry laboratories at the IAMC–CNR Institute of Naples (Italy). The acidification of samples was performed at 50 °C. An internal standard (Carrara Marble with $\delta^{18}O = -2.43$‰ versus Vienna Pee Dee Belemnite [VPDB] and $\delta^{13}C = 2.43$‰ versus VPDB) was run every six samples while the NBS19 international standard was measured every thirty samples. Standard deviations of carbon and oxygen isotope measurements were estimated at 0.1‰ and 0.08‰, respectively, on the basis of replicate measurements of 20% of the analysed samples. All of the stable isotope data are reported in per mil (‰) relative to the VPDB standard (Appendix A).

3.3. Magnetic susceptibility and environmental magnetism

Magnetic susceptibility and environmental magnetism analyses (e.g., Thompson and Oldfield, 1986; Verosub and Roberts, 1995; Evans and Heller, 2003; Liu et al., 2012) were completed at the National Oceanography Centre, Southampton (NOCS), University of Southampton (UK). The χ was measured with a Kappabridge KLY–4 magnetic susceptibility meter (Appendix B). Artificial remanences, including the anhysteretic remanent magnetization (ARM) imparted in a 100 mT AF, with a superimposed 0.05 mT

direct current (DC) bias field, the isothermal remanent magnetization (IRM) imparted in a field of 0.9 T, and back–field demagnetization of the IRM at 0.1 T and 0.3 T were also measured. These data were used to determine the S–ratio300 (IRM–0.3T/IRM0.9T) and the HIRM300 (HIRM = [IRM0.9T + IRM–0.3T] / 2). Natural and artificial remanences were measured using a 2G Enterprises automated pass-through cryogenic magnetometer (Model 755R) with in-line AF demagnetization capability. Environmental magnetic properties (concentration, composition, and dimension of magnetic grains) were defined by investigating ARM, IRM and other indirect parameters (Appendix A). ARM magnetically excites only finer magnetic minerals, while IRM excites all magnetic minerals (concentration). Backfield magnetizations allow us to define HIRM300 and S–ratio300, which give information about coercivities (composition) of the magnetic minerals (Appendix A). Subsamples were analysed with a vibrating sample magnetometer (VSM, MicroMag™ 3900) to measure hysteresis parameters, isothermal remanent magnetization (IRM) acquisition curves and first-order reversal curves (FORCs) at the Instituto Oceanográfico of the Universidade de São Paulo (Brazil). Samples were measured with 80 scaled steps in progressively larger fields until the IRM increased to a saturation IRM (SIRM) in a maximum field of 1.7 T. Coercivity spectra were evaluated from IRM acquisition curves (Robertson and France, 1994) with cumulative log-Gaussian component functions using the software of Kruiver et al. (2001). Magnetic components are characterized by the SIRM, peak field at which half of the SIRM is reached (B1/2), and the dispersion parameter (DP). High-resolution FORC diagrams (Pike et al., 1999; Roberts et al., 2000) were made for representative samples. In order to improve the signal-to noise ratio of FORC measurements, samples were measured multiple times (15 repetitions) and the FORC distributions averaged (Heslop and Roberts, 2012). For FORC measurements, four samples were measured with an averaging time of 200 ms. FORC diagrams were produced with a smoothing factor (SF) of 5 (Roberts et al., 2000) using the algorithm of Heslop and Roberts (2012). The measurement parameters specified by Egli et al. (2010) for resolving central ridge features were used (Hc1 = 0 mT, Hc2 = 110 mT; Hu1 = −15 mT, Hu2 = +15 mT; δH = 0.63 mT).

3.4. Microfossils

3.4.1. Calcareous nannofossils

Samples were prepared from unprocessed material as smear slides and were examined using a light microscope at 1250× magnification. As for biostratigraphy, all samples were studied with a quantitative analysis performed on thirty-one selected samples. In this study, the calcareous nannofossil zonations of Martini (1971) and Okada and Bukry (1980) were applied. Nannofossils were counted using the methods described by Backman and Shackleton (1983) and Rio et al. (1990) counting species versus total assemblage, taking into account at least 300 nannofossils (Appendix C, Appendix D). In order to infer probable temperature and trophic variations of the surface waters, most calcareous nannofossils were, whenever possible, allocated into groups of environmental affinities, largely following Haq and Lohmann (1976), Aubry (1992), Gardin and Monechi (1998), Bralower (2002), Tremolada and Bralower (2004), Persico and Villa (2004), Gibbs et al. (2006), and Raffi et al. (2009). Thus, according to the aforementioned literature, the following environmental groups have been used: warm (Coccolithus pelagicus, Discoaster, Discoasteroides, Ericsonia, Fasciculithus, Heliolithus, Sphenolithus), cold (Chiasmolithus, Cruciplacolithus, Prinsius, Toweius), eutrophic (Chiasmolithus, Cruciplacolithus, Prinsius), mesotrophic (Toweius), meso-oligotrophic (Heliolithus), and oligotrophic (Coccolithus pelagicus, Discoaster, Discoasteroides, Ericsonia, Fasciculithus, Sphenolithus).

3.4.2. Foraminifera

Samples were treated following the cold acetolyse technique of Lirer (2000) by sieving through a 63 μm mesh and drying at 50 °C. The cold acetolysis method enabled extraction of generally easily identifiable foraminifera even from indurated limestones. This technique offered the possibility of accurate taxonomic determination and detailed analysis of foraminiferal assemblages. All samples were studied for biostratigraphical and quantitative analyses. A representative split of at least 300 specimens was picked from the >63 μm fraction, mounted on micro-slides for permanent record and identification purposes, and taxonomically classified at the genus level. However, for the Igorina genus, a species-level classification was adopted following the taxonomic and morphological criteria of Petrizzo (2005). Following Hancock and Dickens (2005), the FI has been calculated using at least 300 specimens and including the whole test, fragments and dissolved tests for estimating the effect of carbonate dissolution (Appendix E). The planktonic foraminiferal zonation of Wade et al. (2011) was followed. Inferred life strategies, environmental affinities and depth ranking of the Paleocene planktonic foraminifera, which derived from latitudinal distribution, environmental inferences (morphology and biogeographic distribution) and stable isotope data, are from Luciani et al. (2007) and references therein. A quantitative study of thirty–four

selected samples was performed. A representative split of the >63 μm fraction was used to pick approximately 300 specimens. The >63 μm fraction was chosen because it can be regarded as the most appropriate for the investigation of the benthic community and because following Schroeder et al. (1987) the study of larger fractions would not be suitable for accurately inferring environmental variations. The sample–split weight used to pick benthic foraminifera was determined so that the foraminiferal density (FD), expressed as the number of foraminifera per gram of dry sediment, could be calculated. The planktonic to planktonic and benthic (P/P + B) ratio, expressed as a percentage, and the percentages of agglutinans and the opportunistic "disaster species" Spiroplectammina spp. were also calculated. In order to calculate the infaunal percentages all taxa were allocated to infaunal and epifaunal morphogroups largely following Corliss (1985), Alegret et al. (2003) and Kaminski and Gradstein (2005). The entire >63 μm residue obtained for all the samples was dried and weighed. The weight percent ratio of the >63 μm size fraction to the weight of the bulk sample (~100 g for each sample) is here referred to as the coarse fraction according to Broecker and Clark, 1999, Broecker and Clark, 2001 (Appendix A). This index, calculated instead using the >38 μm size fraction, has been largely used as a possible indicator of dissolution (i.e., Hancock and Dickens, 2005; Colosimo et al., 2006; Leon-Rodriguez and Dickens, 2010; Luciani et al., 2010). Here we use terminology of Lowest Occurrence (LO) and Highest Occurrence (HO) to delineate the appearance and disappearance of taxa in the section. All the materials studied are housed in the laboratory of the Dipartimento di Dipartimento di Scienze Pure e Applicate, Università di Urbino (Italy).

4. Results

4.1. Magnetobiostratigraphy

On the basis of previous findings of Coccioni et al., 2012, Coccioni et al., 2013, Coccioni et al., 2016, several calcareous nannofossil and planktonic foraminiferal events were recognized in the studied segment as well as just below and above it. They are as follows: LOs of Morozovella occlusa and Morozovella velascoensis (16 m), LO Globanomalina pseudomenardii (17 m), highest occurrence (HO) of Parasubbotina variospira (17.5 m), LO of Heliolithus cantabriae (18 m), LO of Sphenolithus anarrhopus (19.4 m), LO of H. kleinpellii (20.6 m), LO Discoasteroides bramlettei (21 m), LOs of Discoaster mohleri and Heliolithus bukry (23 m), and LO of Acarinina soldadoensis (24 m). The LO of H. cantabriae predates the LO of H. kleinpellii, but a transitional–intergraded form between them has been observed that sometimes hampers the correct identification of these two species (Appendix C, Appendix D). The LOs of H. kleinpellii and D. mohleri define the bases of calcareous nannofossil Zones NP6 and NP7 of Martini (1971), respectively, which correspond to the lower zonal boundaries of Zones CP5 and CP6 of Okada and Bukry (1980). The LO of G. pseudomenardii, the HO of P. variospira and the LO of A. soldadoensis mark the bases of planktonic foraminiferal Zones P4a, P4b and P4c of Wade et al. (2011), respectively. Therefore, the 18–22 m studied segment spans from the planktonic foraminiferal Zone P4b to the upper part of Zone P4b of Wade et al. (2011) and from the lower part of calcareous nannofossil Zone NP5 to the middle part of NP6 of Martini (1971), that is from the lower part of Zone CP4 to the middle part of Zone CP5 of Okada and Bukry (1980) (Fig. 2).

The magnetostratigraphic data enable us to define the base and top of Chron C26n at 16.58 m and 22.4 m, respectively (Fig. 2). This magnetozone is consistently divided in subchrons as recorded in the Contessa Highway section (Lowrie et al., 1982). The 5.82-m thick of C26n at the Contessa Road section is comparable with those of Contessa Highway (ca. 5 m) and Bottaccione (ca. 6 m) sections and at Smirra Core (ca. 3.5–5 m) whose magnetostratigraphies were analysed by Lowrie et al. (1982), Roggenthen and Napoleone (1977) and Turtù et al. (2017), respectively. Because of mismatches with bioevents, the interpretation of C26n might not be fully reliable. In light of it, the Selandian-Thanetian boundary corresponding to the base of magnetochron C26n (Schmitz et al., 2011) was dashed from the inferred base of the C26n up to the LO of D. mohleri.

4.2. CaCO3 content, δ13C and δ18O isotopes and rock magnetic records

The calcium carbonate content record ranges between ~69.2% and ~99.2%, at 20.85 m and 17 m, respectively (Fig. 2). Four discrete intervals containing lower carbonate contents and higher values of χ linked to the marly beds are recognized (Fig. 2). The carbonate δ13C record displays background values of 1.6‰–3.0‰ with three short, distinct negative CIEs at 20.15 m, 20.81 m and 21.88 m, which fall within three discrete marly beds (Fig. 2). However, adjacent limestone and marly limestone beds exhibit similar δ13C values suggesting that these are primarily carbonate signals rather than manifestations of a different lithology. According to Corfield et al. (1991), the Paleogene Scaglia–type sediments near Gubbio might be affected by diagenesis and the oxygen isotope values have, therefore, been disregarded. The

measured carbon isotope values fluctuate around a natural variability range of biogenic calcite precipitated in marine environments so excluding significant effects of burial diagenesis on the carbon isotope signature. Post–depositional carbonate precipitation associated with re-mineralization of organic matter (low carbon isotope values) may influence the δ13C values of the studied bulk sediments. However, the contribution of highly organic-rich sediments in the studied sedimentary context could be reasonably excluded because of the overwhelming dominance of pelagic carbonate.

The rock magnetic properties exhibit marked changes along the studied segment (Fig. 2, Appendix A, Appendix B). Magnetic susceptibility and calcium carbonate records show a significant negative correlation ($r = -0.72$, $p < .01$, $n = 61$). Relatively high values of χ are related to low values of CaCO3 and correspond to peaks in relative abundance of paramagnetic (e.g., increased amount of clay minerals) and ferromagnetic minerals in the sediments. The IRM ranges from 1.81×10^{-5} to 8.93×10^{-4} Am2/kg with an arithmetic mean of 7.49×10^{-5} Am2/kg. The ARM shows an average value of 6.17×10^{-7} Am2/kg (minimum of 1.55×10^{-7} and maximum of 2.35×10^{-6} Am2/kg). The HIRM300 (HIRM = [IRM0.9T + IRM–0.3T] / 2) ranges from 4.99×10^{-6} to 7.51×10^{-4} Am2/kg with an arithmetic mean of 5.00×10^{-5} Am2/kg (Fig. 2). The S-ratio300 (IRM–0.3T/IRM0.9T) varies from 0.27, at 21.60 m, to 1.00 at 20.79–20.87 m with an arithmetic mean of 0.46. The ARM parameter shows spikes with high concentration of finer magnetic grains, whereas IRM activate the entire magnetic component (concentration), and HIRM provides information about the magnetic coercivity of the magnetic carriers. The presence of low coercivity magnetic mineral (i.e., magnetite) is indicated by the value of S-ratio300 close to the unit (20.79–20.87 m). In contrast, low S–ratio300 values and high values of HIRM300 indicate the presence of high-coercivity magnetic minerals (i.e., hematite). The two latter parameters indicate both a subtle variation in the composition of magnetic minerals as well as a significant variation in grain size and concentration. The coarse fraction record shows a marked decrease from 19.3 to 21 m (Fig. 2).

Representative IRM acquisition curves for the studied intervals are shown in Fig. 3 and Table 1. The first component (component 1) with low coercivity range, with B1/2 of approximately 2–21 mT and a wide DP of 0.17–0.41, is present in all samples (Fig. 3a; black curve). Components 2 and 3 in the low coercivity range with B1/2 of ~20–62 mT and characterized by a narrow DP of 0.19–0.29 are also present in all samples (Fig. 3a; green and blue curves, respectively). An intermediate coercivity component (B1/2–158–316 mT; DP ~0.18–0.40; Fig. 3a, yellow curve), and a high-coercivity component (B1/2–1122–1445 mT; DP ~0.10–0.15) are also identifiable in all IRM curves (Fig. 3a; orange curve). FORC diagrams present a marked central horizontal ridge, with coercivity peaks between 20 and 40 mT, and with very limited vertical dispersion (Fig. 4a–d). The sharp vertical peak of the FORC distributions indicates a dominance of single-domain (SD) non-interacting particles.

4.3. Biotic changes

According to Coccioni et al. (2012), the most significant abiotic changes are recorded in the 4-m-thick interval spanning 18–22 m that is therefore here considered for unravelling the biotic changes.

4.3.1. Calcareous nannofossils

Calcareous nannofossils assemblages are not particularly rich and diversified. In most of the studied samples calcareous nannofossils exhibit poor to good preservation, but enhanced dissolution has been observed from 19.2 to 20.95 m based on the preservation criteria proposed by Roth and Thierstein (1972). Assemblages are dominated by Coccolithus pelagicus, Sphenolithus spp. and Toweius spp. (mostly T. pertusus and T. eminens), with subordinate numbers of Fasciculithus spp., Heliolithus spp., and Prinsius spp. (Fig. 5, Appendix C). Populations are dominated by warm-water taxa without marked changes throughout the studied segment and by oligo-mesotrophic taxa (Fig. 5, Appendix C). From 19.2 to 20.95 m, the trophic groups undergo remarkable changes. In particular, the eutrophic indices representing only a minor component of the assemblages exhibit a slight decrease from 19.2 to 20.75 m, the meso-oligotrophic and mesotrophic indices show a concomitant increase that is more pronounced from 20.05 to 20.95 m with the highest values in correspondence of the marly layer at 20.75–20.95 m corresponding to the ELPE equivalent, whereas oligotrophic group displays a sensitive reduction (Fig. 5, Appendix C). The turnover in abundance of H. cantabriae vs. H. kleinpellii that might be used for marking the base of the ELPE equivalent is observed between samples 20.6 m and 20.89 m (Appendix D).

4.3.2. Planktonic foraminifera

The planktonic foraminiferal assemblages are rich and generally well diversified and preserved from 18 to 19.2 m and from 21 to 22 m, where they are mainly composed, in similar proportions, of different representatives of the genera Acarinina, Igorina, Morozovella, Subbotina and Parasubbotina with

subordinate numbers of Chiloguembelina, Zeauvigerina and Globanomalina (Fig. 6, Appendix E). From 19.2 to 20.95 m populations are relatively less diversified and largely dissolved, particularly within the marly layer at 20.75–20.95 m corresponding to the ELPE equivalent. In addition, they exhibit a gradual increase in the relative abundance of Igorina (especially represented by I. tadjikistanensis, I. pusilla "high trochospire" and I. albeari "chubby") and a concomitant gradual decline in the relative abundance of Morozovella, Acarinina, Subbotina and Parasubbotina together with a larger number of Chiloguembelina and Zeauvigerina and a lower number of Globanomalina (Fig. 6, Appendix E). However, according to their relative abundances, Acarinina suffered a minor decline with respect to Morozovella from 19.2 to 20.05 m (Fig. 6, Appendix E). Interestingly, within the ELPE equivalent, Igorina (mainly I. albeari "chubby" and I. tadjikistanensis) peaks in abundance and occurs together with Acarinina that returns to increase in abundance and low numbers of Acarinina, Chiloguembelina, Zeauvigerina, subbotinids, and scattered specimens of Morozovella (Fig. 6, Appendix E). The FI displays a clear increasing trend from 18.6 m to 20.95 m with higher values within the marly layers at 20.05–20.09 m, 20.15–20.17 m and 20.75–20.95 m (up to ~80% at 20.85 m) (Fig. 6, Appendix E).

4.3.3. Benthic foraminifera

The benthic foraminiferal assemblages are generally well diversified and preserved throughout the studied segment, except within the marly layer at 20.75–20.95 m corresponding to the ELPE equivalent where some evidence of dissolution is observed (Fig. 7, Appendix F). Populations are dominated by calcareous-hyaline forms with variable percentages of agglutinans that normally peak in correspondence with the marly layers (Fig. 7, Appendix F). Interestingly, three discrete pulses of Spiroplectammina spp. occur, with increasing percentages, within the marly layers at 20.05–20.09 m, 20.15–20.17 m and 20.75–20.95 m (Fig. 7, Appendix F). Infaunal and epifaunal taxa are present in different proportions within the assemblages. However, epifaunal taxa prevail in most of the samples, with higher percentages from 20.05 to 20.95 m (Fig. 7, Appendix F). The epifaunal taxa first gradually increase in abundance reaching the highest percentage, and then slightly decline just within the marly layer at 20.75–20.95 m, which corresponds also to the highest values of FD. The P/(P + B) ratio fluctuates throughout the studied segment with decreasing values from 19.2 m upwards and lower percentages from 20.05 to 21.3 m. The lowest value (~30%) is found at 20.85 m (Fig. 7, Appendix F). The fluctuations of the P/(P + B) ratio are well mirrored by the FD (Fig. 7, Appendix F).

5. Discussion

5.1. Defining and constraining the age and duration of the STTE and the ELPE equivalent at Contessa Road

Significant changes, both in the surface water and at the seafloor, took place across the studied interval as revealed by several rock parameters and by calcareous nannofossils and foraminifera at the Contessa Road section. On the basis of the biotic and abiotic changes, the 4 m–thick studied segment can be subdivided into five discrete intervals of different durations, as follows: Interval 1 (18–19.2 m, ~240 kyr), Interval 2a (19.2–20 m, ~160 kyr), Interval 2b (20–20.75 m, ~150 kyr), Interval 3 (20.75–20.95 m, ~40 kyr) and Interval 4 (20.95–22 m, ~210 kyr) (Fig. 8). Intervals 2 and 3 are characterized by pronounced changes, which indicate that important, stepwise environmental and ecological perturbations took place during their deposition. In particular, Interval 4, which corresponds to a discrete marly layer, starts just after the evolutionary LO of H. kleinpellii, and falls in the middle part of Zone P4b. The base of this interval marks the turnover between the H. cantabriae and H. kleinpellii abundances that can be used for identifying the onset of the ELPE equivalent. A similar transition occurs at site 1262 (Agnini et al., 2007). In light of it and considering the biostratigraphy, the Interval 3 might be confidently correlated with the ELPE of Bralower et al., 2002, Bralower et al., 2006, Zachos et al. (2004) and Agnini et al. (2007), which would, therefore, be the sedimentary expression of this event at Contessa Road (Fig. 1 SM). Accordingly, this event firstly described by Bralower et al. (2002) at the Shatsky Rise (ODP Sites 1209, 1210, 1211 and 1212) is represented by a prominent 5– to 25 cm–thick clay–rich calcareous nannofossil ooze layer falling in the lower planktonic foraminiferal P4 Zone of Berggren et al. (1995) and coinciding with the evolutionary LO of H. kleinpellii that marks the base of calcareous nannofossil Zones NP6 of Martini (1971) and CP5 of Okada and Bukry (1980). A relationship between the consecutive appearances of the genera Heliolithus, Discoasteroides and Discoaster, and ELPE was demonstrated by Agnini et al. (2007) at Site 1262, with these evolutionary impulses being related to environmental perturbations leading to the onset of the ELPE (the emergence of Heliolithus) and to the critical conditions during (the emergence of Discoasteroides) and after (the emergence of Discoaster) the transient event. In such a scenario, Intervals 2 and 3 would represent the sedimentary expression of a relatively long lasting event that we

here name the Selandian-Thanetian Transition Event (STTE) (Fig. 8). Interval 3, that is the ELPE equivalent, would represent the climax phase of the STTE.

5.2. Carbon isotope and magnetic records of the STTE at Contessa Road

The STTE at Contessa Road is characterized by a decreasing trend in δ13C values with an abrupt negative CIE (~0.6‰) in correspondence with the ELPE equivalent, as well as drops in carbonate content, enhanced carbonate dissolution, and pronounced peaks in χ (Fig. 2, Fig. 8). The amplitude of the CIE shows intermediate values when compared with other sections and sites, namely Zumaia (~1‰), ODP Sites 1262 (~0.3‰) and 1209 (benthic ~0.4‰) (Bernaola et al., 2007; Westerhold et al., 2011; Littler et al., 2014). Two negative organic CIEs (δ13Corg) of ~3‰ and ~4.5‰ were found in the terrestrial record at Cerro Bayo, the former correlated with the MPBE and the second roughly ~300 kyr later (Hyland et al., 2015). The CIE of the ELPE might be ascribed to additions of 13C-depleted carbon into the ocean–atmosphere system from an external carbon reservoir that can be both rapidly assimilated in the carbon cycle (Hyland et al., 2015). This input might have promoted a substantial shoaling of the lysocline, along with an accelerated hydrologic and weathering cycle, like in other hyperthermals (Dickens et al., 1995; Lourens et al., 2005; Nicolo et al., 2007). At Site 1262, this event is marked by rapid negative excursions in benthic δ18O values that was interpreted as a rapid warming of up to ~4 °C (Littler et al., 2014). The same authors suggested a large-scale release of reduced carbon sufficient to cause significant shoaling in the already relatively shallow CCD.

All these changes might be directly evidenced at Contessa Road section by the χ and other magnetic parameters occurring throughout the STTE, with the highest values corresponding with the marly layers and, particularly, within the ELPE equivalent (Fig. 2, Fig. 8). The S-ratio300 values close to the unit suggest that the most abundant magnetic mineral is magnetite. On the other hand, the presence of hematite is indicated by low S-ratio300 values and high values of HIRM300. The χ variations may be due to the changes in the concentration of mainly ferromagnetic and subordinately paramagnetic minerals, which could be related to changes in terrigenous influx, carbonate dissolution or magnetic mineralogy, which in turn might be related to redox conditions on the seafloor – low coercivity (i.e., magnetite) vs. high coercivity magnetic minerals (i.e., hematite) - or to the nature of the weathering in the continental search area (Jovane et al., 2004). Previous studies show that terrigenous material was transported into the Umbria-Marche basin mainly by wind (Arthur and Fischer, 1977; Johnsson and Reynolds, 1986; Sinnesael et al., 2016). Paleogeographic reconstructions show that Umbria-Marche was a deep marine basin and the continental landscapes were >500 km away, excluding the hypothesis of fluvial source for terrigenous material (Dercourt et al., 1993; Adatte et al., 2002; Rosenbaum et al., 2002). Variations in magnetic susceptibility and Fe content, which reflect changes in clay contents, have been documented during prominent events (i.e., K/Pg, ELPE, PETM) both in the Pacific and Atlantic oceans (Westerhold et al., 2008; Hilgen et al., 2010). These changes appear to be controlled by carbonate dissolution (Zachos et al., 2003; Hancock and Dickens, 2005) driven by the expansion and contraction of biosphere productivity in response to changes in solar insolation (Pälike et al., 2006). At the deep sites of Walvis Ridge and Shatsky Rise, a lowering of sedimentation rate was documented during the ELPE and its equivalents that might be related to changes in productivity and/or preservation (Westerhold et al., 2008). The higher sedimentation rate at the shallower Atlantic ODP Site 1051 and the condensed sequences at Shatsky Rise confirm lysocline shoaling during the ELPE and its equivalents (Westerhold et al., 2008). Moreover, on the basis of the planktonic/benthic ratio and the percentages of planktonic foraminiferal fragments or partially dissolved tests (fragmentation index, FI), Hancock and Dickens (2005) extended the dissolution interval at Sites 1209 and 1211 beyond the biotic event previously defined by Petrizzo (2005) and highlighted that the event marks a short extreme within the context of a longer 1–2 My interval of odd conditions. This supports the hypothesis of a prominent change in ocean circulation as also corroborated by the occurrence of an unusual black shale-condensed interval at Mead Stream, found within the Waipawa Formation deposited under dysaerobic conditions and surface-water warming (Killops et al., 2000), falling within Zone P4 of Berggren et al. (1995) and correlated throughout New Zealand (Hollis et al., 2005).

5.3. Magnetotactic bacteria

Magnetotactic bacteria (MTB) produce intracellular biogenic magnetite, called magnetosome, to find the ideal redox-oxic conditions into sediments (Bazylizinki et al., 1993). In particular conditions, magnetosome can be preserved during sediment diagenesis and, finally, maintain a stable and single domain (SD) magnetization (Roberts et al., 2011, Roberts et al., 2013; Jovane et al., 2012).

The coercivity and DP of component 1 of the IRM acquisition might suggest the presence of detrital iron oxides (e.g., Maher, 1988; Moskowitz et al., 1989; Kruiver et al., 2001; Egli, 2004; Font et al., 2011, Font et al., 2014; Savian et al., 2014), whereas those of components 2 and 3 are indicative of SD biogenic soft (BS) and biogenic hard (BH) magnetic particles produced by MTB (Kruiver and Passier, 2001; Egli, 2004; Yamazaki, 2012). Ancient sediments also show these components (Abrajevitch and Kodama, 2009, Abrajevitch and Kodama, 2011; Larrasoaña et al., 2012; Roberts et al., 2013; Abrajevitch et al., 2014; Heslop et al., 2014; Savian et al., 2014, Savian et al., 2016), which can be different in terms of median coercivity due to differences in magnetosome morphology (Egli, 2004; Jovane et al., 2012; Yamazaki, 2012; Chang et al., 2012; Heslop et al., 2014). The high-coercivity of component 5 suggests the presence of hematite (Kruiver et al., 2001; Abrajevitch et al., 2009; Savian et al., 2014), but cannot also exclude some fraction of goethite due to the similar coercivity. The FORC distributions provide evidence of enhanced magnetofossils during the STTE event (Fig. 4c). The narrow vertical spread and a so-called central ridge feature of the FORC distributions indicate a dominance of SD non-interacting particles and are characteristic of intact magnetosome chains (Roberts et al., 2000; Egli et al., 2010). The Pre- and Post-STTE (Fig. 4a, d) FORC distributions show results typical of detrital magnetite with vertical peak of the FORC distribution below 20 mT. Therefore, the increasing bulk magnetization of the sediments at Contessa Road section observed during the STTE is also related to an increase of MTB productivity.

During the STTE event at Contessa Road section, nutrients show a shift towards mesotrophic conditions, also coincident with increased hematite and magnetofossils concentrations (Roberts et al., 2011; Savian et al., 2014). The increased hematite concentrations could be attributed to a major influx of aeolian dust mainly produced in desert lands (Upchurch et al., 1999; Hunter et al., 2013), probably sourced from the north-western corner of Africa and South Asia (e.g., Dercourt et al., 1993; Hay et al., 1999). The aeolian dust flux might have brought limiting micronutrients, including iron, to surface waters that stimulated the primary productivity. The iron fertilization associated with aeolian dust flux would have stimulated and then increased the primary productivity (Roberts et al., 2011). This source of iron under diagenetic iron reducing sedimentary conditions is also responsible to have enhanced MTB productivity. Generally, hyperthermal events are associated to enhanced hydrological cycle and chemical weathering, whereas a higher input of aeolian dust requires dry climatic conditions. On the other hand, distinct increasing biogenic magnetic signals coupled with increasing fertility were observed. This pattern suggests the presence of arid climatic zones at regional scale. Alternatively, significant changes in water circulation could have delivered more nutrients into the Tethys in some periods (Jovane et al., 2009), which could also have re-defined the oxygen minimum zone (OMZ) and stimulated the primary and the MTB productivity. In this case, the presence of hematite in the sediments can be due to the partial oxidation of the magnetosomes (Rodelli et al., 2018).

5.4. Reading the biotic changes induced by the STTE at Contessa Road: which scenario for this environmental perturbation?

The remarkable changes in the relative abundances, preservation, and taxonomical composition of calcareous nannofossil and foraminiferal assemblages show that during the STTE, and particularly in correspondence with the ELPE equivalent, these changes appear to be more prominent. An abrupt environmental perturbation took place both in the photic zone and at the seafloor following a period of relatively stable environmental conditions characterized by essentially warm and oligotrophic surface waters (Fig. 5, Fig. 6, Fig. 7, Fig. 8). Although the response of calcareous nannofossils to multiple environmental factors is fairly complex and still largely unclear (i.e., Raffi et al., 2009), the increase in abundance of the meso-oligotrophic to mesotrophic taxa and the concurrent decrease of oligotrophic ones might indicate slightly more trophic conditions during the STTE (Intervals 2 and 3), with more nutrients availability in correspondence of the ELPE equivalent (Interval 3) (Fig. 5, Fig. 8).

Higher FI and lower P/(P + B) ratio values during the STTE (Fig. 5, Fig. 6, Fig. 8) strongly reflect the effect of enhanced carbonate dissolution, most likely driven by a shallowing of the lysocline caused by acidification of the oceans as also identified at Shatsky Rise (Hancock and Dickens, 2005). These conditions reach their climax during the ELPE equivalent, where impoverished and largely dissolved planktonic foraminiferal assemblages also occur as documented in other records, namely Shatsky Rise (Petrizzo, 2005) and Walvis Ridge (Zachos et al., 2004).

The generally well diversified and preserved planktonic foraminiferal assemblages of interval 1 are replaced by a gradually less diversified, largely dissolved and Igorina (predominantly represented by I. tadjikistanensis, I. pusilla “high trochospire” and I. albeari “chubby”) dominated ones, particularly within the marly layer corresponding to the ELPE equivalent. These changes were accompanied by a gradual decline in the relative abundance of Morozovella, Acarinina, Subbotina and Parasubbotina together with a

larger number of Chiloguembelina and Zeauvigerina (Fig. 6). Similar variations were documented at Shatsky Rise and at Walvis Ridge records (Zachos et al., 2004; Petrizzo, 2005).

The genera Igorina, Acarinina and Morozovella have widely been inferred to be oligotrophic, warm-water surface-dweller taxa (i.e., Luciani et al., 2007 and references therein). Among these genera, the symbiont-bearing Igorina, which is believed to have occupied a depth habitat between the shallower photosymbiotic morozovellids and the relatively deeper photosymbiotic acarininids, might have benefited the most from the changing environmental conditions during the STTE, most likely replacing the ecological niches vacated by Acarinina, Globanomalina, Morozovella and subbotinids. However, according to their relative abundances, Acarinina suffered a minor decline with respect to Morozovella in the early phase (Interval 2) of the STTE and partially recovered during the ELPE equivalent (Fig. 6). It cannot be excluded, therefore, that in this phase the ecological niches vacated by the morozovellids were firstly filled by the acarininids in agreement with a similar life strategy documented by Luciani et al. (2007) and Agnini et al. (2009) during the PETM and the K hyperthermal events. The dominance of I. tadjikistanensis, I. pusilla “high trochospire” and I. albeari “chubby” during the STTE could be interpreted as a morphologic response to a relative change in surface water productivity, which enhanced species competition forcing the igorinids to modify their morphologies to cope. Subbotina, Parasubbotina and Globanomalina are considered opportunistic genera that prefer deeper, colder and more eutrophic waters (i.e., Luciani et al., 2007 and references therein). Their decline in abundance during the STTE might be essentially driven by ecological competition and differential dissolution, the latter probably more significant since Subbotina and Parasubbotina are known to be prone to that process (i.e., Luciani et al., 2007 and references therein). The increase in abundance of the opportunistic, intermediate dwellers Chiloguembelina and Zeauvigerina that thrive in low-oxygen environments (i.e., Luciani et al., 2007 and references therein) during the STTE, may document a weakly developed oxygen minimum zone in the depositional environment of that time (Fig. 6, Fig. 8). Moreover, the slight increase in Acarinina, a meso-oligotrophic genus, and low-oxygen tolerant Chiloguembelina and Zeauvigerina along with the drop in abundance of the oligotrophic morozovellids during the ELPE equivalent might be interpreted as a slight increase in the trophic levels. This scenario is consistent both with the suggestion of Agnini et al. (2009) for the K event at Farra, where the surface dwelling acarininids were able to temporarily proliferate in nutrient enriched waters previously occupied by subbotinids and to better tolerate these conditions than morozovellids.

The relatively higher numbers of the benthic agglutinated foraminifera in correspondence with the marly layers within the STTE could further support the presence of dissolution, probably induced by shallowing of the lysocline (Fig. 7, Fig. 8). From our data no clear sign of oxygen deficiency at the seafloor has been documented at the Contessa Road section. The higher abundance of epifaunal taxa during the STTE might be interpreted as a lowering of nutrient availability at the seafloor but in agreement with the calcareous plankton data, differential dissolution probably played a major role in determining lowered values of the epifauna to infauna ratio (Fig. 7, Fig. 8) (Frontalini et al., 2016). Following Herguera and Berger (1991), the higher values of FD during the STTE and particularly during the ELPE equivalent might suggest enhanced food supply at the seafloor, but a complex interplay of increasing and differential dissolution susceptibility in planktonic foraminifera when compared to their benthic counterparts cannot be ruled out (Hancock and Dickens, 2005). The increase of benthic relative to planktonic foraminifera during the ELPE has been also documented at Shatsky Rise (ODP Site 1209), and Zumaia and Río Gor sections (Petrizzo, 2005; Bernaola et al., 2007; Pujalte et al., 2014). Moreover, the marked changes affecting the planktic ecosystem might have determined changes in quality and quantity of the food flux to the seafloor, thus triggering changes in the benthic communities. Finally, the occurrence of marked peaks in abundance Spiroplectammina, which is known to be an opportunistic “disaster taxon” indicating a stressed environment (Kuhnt and Kaminski, 1996), would mark significant environmental disturbance at the seafloor, in particular in correspondence of the ELPE equivalent (Fig. 7, Fig. 8).

The ecological disruption related to the STTE has been more severe in the later phase of that event (Interval 2b), and particularly during the ELPE equivalent (Interval 3), which can be considered the climax of the STTE. At the end of the STTE (Interval 4), a rapid environmental and ecological recovery occurs, with the relative abundances, preservation and composition of the main components of calcareous nannofossil and foraminiferal assemblages moving towards features similar to those of the pre-STTE conditions (Interval 1). Interestingly, no major biotic extinctions occurred among calcareous nannofossils and foraminifera during the STTE, even though it represents a significant event inducing severely stressed surface water and seafloor environments. In particular, the complex interplay of the enhancing surface productivity and dissolution, which involved changes in relative abundances, preservation and composition of primary producers (calcareous nannoplankton) and zooplankton (planktonic foraminifera), may have been affected by the reorganization of the planktic ecosystem. These changes may have, in turn, altered the food flux (i.e., type and quantity) to the seafloor, thus triggering changes in the benthic

communities. The biotic and abiotic variations that took place during the STTE indicate gradual changes in paleoenvironmental conditions rather than a sudden event both in the photic zone and at the seafloor. These major changes suggest a scenario characterized by an enhanced nutrient availability during the STTE, which peaks during the ELPE equivalent. Significant changes in terms of rapid negative excursions in benthic δ18O has been documented at ODP Site 1262, where a rapid warming of up to ~4 °C above the Late Paleocene background temperatures of ~8 °C has been inferred (Littler et al., 2014). On the other hand, no significant changes have been found through the high-resolution benthic foraminiferal stable isotope record of the ODP Site 1209, where slight increasing values of δ18O, probably accompanied by a small decrease in temperature, and a complex δ13C record have been detected across the ELPE (Westerhold et al., 2011). The findings of ODP site 1209 seem to be in agreement with the Contessa Road data, where no significant changes in paleotemperature as inferred from calcareous nannofossil assemblages have been found.

5.5. A long-lasting environmental disruption during middle-early late Paleocene

The variations in the planktonic foraminiferal assemblages recognized before (Intervals 2a and 2b), during (Interval 3) and after (Interval 4) the deposition of the marly layer equivalent to the ELPE (Fig. 6) well mirror those recorded before, during, and after the ELPE at Shatsky Rise by Petrizzo (2005) and also support the suggestion of Hancock and Dickens (2005) that the ELPE at Sites 1209 and 1211 might have marked only a short period within the context of a 1–2 Myr long interval of unstable conditions. Furthermore, a prolonged ELPE interval of enhanced calcareous nannofossil dissolution was observed at site 1262 by Agnini et al. (2007).

Interestingly, the comparison of biostratigraphic and biotic records between Tethyan sections, such as Zumaia and the Contessa Road section, and the deep-sea cores, shows mismatches and uneven biotic response. In fact, according to Bernaola et al. (2007), the ELPE equivalent is placed well after (~273 kyr based on cycle-counting) the LO of H. kleinpellii and in the upper part of C26r (~168 kyr prior the Chron C26r/C26n boundary). Moreover, within the planktonic foraminiferal assemblages of the core of the ELPE equivalent, Igorina declines while Subbotina largely and concurrently increases in abundance. Therefore, the biotic response of the planktonic foraminiferal assemblages of the ELPE equivalent at Zumaia is significantly different from those documented at Contessa Road, Shatsky Rise and Walvis Ridge. This different biotic response could reflect a different depositional setting and the biochronostratigraphic discrepancy might be explained by the occurrence of transitional forms (intergrades) between H. kleinpellii and its ancestor H. cantabriae, which sometimes may hamper precise identification (Agnini et al., 2007). Moreover, the pinpointing of the precise position of Chron C26n in deep-sea cores is hampered by its proximity to the ELPE (Röhl et al., 2004; Bralower et al., 2006; Westerhold et al., 2008). All of these data and remarks from different ocean and land-based sites suggest that the scenario at the Selandian-Thanetian transition is not just perturbed by a minor hyperthermal event, as previously thought, but is characterized by few hundreds of kyrs of highly climatic and oceanographic variability. This produced dissimilar conditions, with possibly even opposite patterns, in different oceanic basins at regional scale.

6. Conclusions

Detailed analyses of calcareous nannofossils and foraminiferal assemblages, and high-resolution geochemical, isotopic and magnetic records across the Selandian-Thanetian transition at Contessa Road (Gubbio, Italy) allow us to recognize and accurately document a 350-kyr-lasting interval of environmental perturbations that we here name the Selandian-Thanetian Transition Event (STTE). These changes clearly outline a long-lasting paleoenvironmental evolution in the western central Tethys across the Selandian-Thanetian transition. The Contessa Road represents the first land-based section where the STTE is recognized and its paleoenvironmental effects documented. The remarkable changes in the relative abundances, preservation and composition of calcareous nannofossils and foraminiferal assemblages show that during the STTE a marked environmental perturbation took place and reached its climax during the ELPE equivalent. During the STTE and, particularly, the ELPE, have been recognized the presence of magnetofossils that is somehow related to increase of primary productivity in warm climate conditions. The environmental instability was not confined within the photic zone but extended to the seafloor resulting in little more trophic conditions of the sea surface waters with an enhanced, but of reduced extent, nutrient availability on the seafloor under almost unchanged warm-water conditions and marked rise of lysocline. This enhanced fertilization also promotes magnetotactic bacterial development. It remains to be understood whether the STTE represents a regional or global event. The comparison of

biotic and abiotic records throughout the STTE at Contessa Road section with available data across the ELPE from former investigated ocean and land-based sites provides lines of evidence that this latter event might be indeed only the terminal part of a long-lasting environmental change than hitherto supposed.

Acknowledgments

The authors are grateful to the Editor Thierry Corrège and three anonymous reviewers for their thoughtful and valuable comments that have greatly improved the manuscript. We also warmly thank Sandro Montanari for his suggestions and comments. Luigi Jovane is funded from Marie Curie Actions (FP7-PEOPLE-IEF-2008 proposal n. 236311) and Fundação de Amparo à Pesquisa do Estado de São Paulo (FAPESP) processo n. 2011/22018-3. This study was financed in part by the Coordenação de Aperfeiçoamento de Pessoal de Nível Superior - Brasil (CAPES) - Finance Code 001 and Ciências do Mar II. Jairo Savian thanks the Paleomagnetic Laboratory of National Oceanography Centre Southampton (NOCS) for the use of equipment facilities and Conselho Nacional de Desenvolvimento Científico e Tecnológico (CNPq – grant 201508/2009 5) for the scholarship. Jairo Savian also acknowledges Fundação de Amparo à Pesquisa do Estado do Rio Grande do Sul (FAPERGS) for financial support through grant 16/2551-0000213-4. We warmly thank Carla Bucci for her technical support. The research for this paper was partially made possible by the financial support from the Dipartimento di Scienze Pure e Applicate (DiSPeA) to FF and RC.

References

A. Abrajevitch, K. KodamaBiochemical vs. detrital mechanism of remanence acquisition in marine carbonates: a lesson from the K-T boundary interval Earth Planet. Sci. Lett., 286 (2009), pp. 269-277

Abrajevitch, A., Kodama, K., 2011. Diagenetic sensitivity of paleoenvironmental proxies: a rock magnetic study of Australian continental margin sediments. Geochem. Geophys. Geosyst. 12, Q05Z24. doi:10.1029/2010GC003481

A. Abrajevitch, R. Van der Voo, D.K. ReaVariations in relative abundances of goethite and hematite in Bengal Fan sediments: climatic vs. diagenetic signals Mar. Geol., 267 (2009), pp. 191-206

A. Abrajevitch, A.P. Roberts, K. KodamaVolcanic iron fertilization of primary prductivity at Kerguelen Plateau, Southern Ocean, through the Middle Miocene Climate Transition Palaeogeogr. Palaeoclimatol. Palaeoecol., 410 (2014), pp. 1-13, 10.1016/j.palaeo.2014.05.028

T. Adatte, G. Keller, W. StinnesbeckLate Cretaceous to early Paleocene climate and sea-level fluctuations: the Tunisian record Palaeogeogr. Palaeoclimatol. Palaeoecol., 178 (2002), pp. 165-196, 10.1016/S0031-0182(01)00395-9

C. Agnini, E. Fornaciari, I. Raffi, D. Rio, U. Rohl, T. WesterholdHigh-resolution nannofossil biochronology of middle Paleocene to early Eocene at ODP Site 1262: implications for calcareous nannoplankton evolution Mar. Micropaleontol., 64 (2007), pp. 215-248

Agnini, C., Macrì, P., Backman, J., Brinkhuis, H., Fornaciari, E., Giusberti, L., Luciani, V., Rio, D., Sluijs, A., Speranza, F., 2009. An early Eocene carbon cycle perturbation at ~52.5 Ma in the Southern Alps: chronology and biotic response. Paleoceanography 24, PA2209. doi:https://doi.org/10.1029/2008PA001649.

L. Alegret, E. Molina, E. ThomasBenthic foraminiferal turnover across the Cretaceous/Paleogene boundary at Agost (southeastern Spain): paleoenvironmental inferences Mar. Micropaleontol., 48 (2003), pp. 251-279

M.A. Arthur, A. FischerUpper Cretaceous–Paleocene magnetic stratigraphy at Gubbio Italy. I. Lithostratigraphy and sedimentology. Geol. Soc. Am. Bull., 88 (1977), pp. 367-371, 10.1130/0016-7606(1977)88<367:UCMSAG>2.0.CO;2

M.-P. AubryLate Paleogene calcareous nannoplankton evolution: a tale of climatic deterioration, D.R. Prothero, W.A. Berggren (Eds.), Eocene-Oligocene Climatic and Biotic Evolution: Princeton, Princeton University Press, New Jersey (1992), pp. 272-309

J. Backman, N.J. ShackletonQuantitative biochronology of Pliocene and early Pleistocene calcareous nannofossils from the Atlantic, Indian and Pacific oceans Mar. Micropaleontol., 8 (1983), pp. 141-170

D.A. Bazylizinki, B.R. Heywood, S. Mann, R.B. Frankel Fe304 and Fe3S4 in a bacterium Nature, 366 (1993), p. 218

Berggren, W.A., Kent, D.V., Swisher, C.C., Aubry, M.P., 1995. A revised Cenozoic geochronology and chronostratigraphy. In: Berggren, W.A., Kent, D.V., Swisher III, C.C., Aubry, M.P. (Eds.), Geochronology, Time and Global Stratigraphic Correlation, Special Publication-Society of Economic Paleontologist and Mineralogist, 54. SEPM (Society for Sedimentary Geology), Tulsa, OK, pp. 129–213.

G. Bernaola, J.I. Baceta, X. Orue-Extebarria, L. Alegret, M. Martin-Rubio, J. Arostegui, J. Dinarès-TurellEvidence of an abrupt environmental disruption during the mid-Paleocene biotic event (Zumaia section, western Pyrenees) Geol. Soc. Am. Bull., 119 (2007), pp. 785-795

G.J. Bowen, D.J. Beerling, P.L. Koch, J.C. Zachos, T. QuattlebaumA humid climate state during the Palaeocene/Eocene thermal maximum Nature, 432 (2004), pp. 495-499

T.J. BralowerEvidence of surface water oligotrophy during the Paleocene-Eocene thermal maximum: nannofossil assemblage data from Ocean Drilling Program Site 690 Maud Rise: Weddell Sea: Paleoceanography, 17 (2002), p. 1023, 10.1029/2001PA000662

T.J. Bralower, I. Premoli Silva, M.J. MaloneNew evidence for abrupt climate change in the Cretaceous and Paleogene: an Ocean Drilling Program expedition to Shatsky Rise, northwest Pacific Geol. Soc. Am. Today, 12 (2002), pp. 4-10

T.J. Bralower, I. Premoli Silva, M.J. MaloneLeg 198 synthesis: a remarkable 120-m.y. record of climate and oceanography from Shatsky Rise, northwest Pacific Ocean. In: Bralower, T.J., Premoli Silva, I., and Malone, M.J. (Eds.), Proc. ODP, Sci Results, 198 (2006), pp. 1-47

W.S. Broecker, E. ClarkCaCO3 size distribution: a paleocarbonate ion proxy? Paleoceanography, 14 (1999), pp. 596-604

W.S. Broecker, E. Clark Re-evaluation of the CaCO3 size index paleocarbonate ion proxy Paleoceanography, 16 (2001), pp. 669-671

L. Chang, A.P. Roberts, W. Williams, J.D. Fitz Gerald, J.C. Larrasoaña, L. Jovane, A.R. MuxworthyGiant magnetofossils and hyperthermal events Earth Planet. Sci. Lett., 351–352 (2012), pp. 258-269

L. Chang, R.J. Harrison, F. Zeng, T.A. Berndt, A.P. Roberts, D. Heslop, C. Zhao Coupled microbial bloom and oxygenation decline recorded by magnetofossils during the Paleocene-Eocene Thermal Maximum Nat. Commun., 9 (1) (2018), p. 4007

R. Coccioni, F. Frontalini, G. Bancalà, E. Fornaciari, L. Jovane, M. SprovieriThe Dan-C2 hyperthermal event at Gubbio (Italy): global implications, environmental effects, and cause(s) Earth Planet. Sci. Lett., 297 (2010), pp. 298-305

R. Coccioni, G. Bancalà, R. Catanzarit, E. Fornaciari, F. Frontalini, L. Giusberti, L. Jovane, V. Luciani, J. Savian, M. SprovieriAn integrated stratigraphic record of the Palaeocene–lower Eocene at Gubbio (Italy): new insights into the early Palaeogene hyperthermals and carbon isotope excursions Terra Nova, 24 (2012), pp. 380-386, 10.1111/j.1365-3121.2012.01076.x

R. Coccioni, M. Sideri, G. Bancalà, R. Catanzariti, F. Frontalini, L. Jovane, A. Montanari, J. SavianIntegrated stratigraphy (magneto-, bio-and chronostratigraphy) and geochronology of the Palaeogene pelagic succession of the Umbria-Marche Basin (central Italy) L. Jovane, E. Herrero-Bervera, L.A. Hinnov, B.A. Housen (Eds.), Magnetic Methods and the Timing of Geological Processes, Geol. Soc. Lond. Spec. Publ, vol. 373 (2013), pp. 111-131, 10.1144/SP373.4

Coccioni, R., Catanzariti, R., Frontalini, F., Galbrun, B., Jovane, L., Montanari, A., Savian, J., Sideri, M., 2016. Integrated magnetostratigraphy, biostratigraphy, and chronostratigraphy of the Paleogene pelagic succession at Gubbio (central Italy). In: Menichetti, M., Coccioni, R., and Montanari, S., (Eds.), The Stratigraphic Record of Gubbio: Integrated Stratigraphy of the Late CretaceousPaleogene UmbriaMarche Pelagic Basin. Geol. Soc. Am. Bull. Spec. Paper 524, 139–160. doi:https://doi.org/10.1130/2016.2524(10).

A.B. Colosimo, T.J. Bralower, J.C. ZachosEvidence of lysocline shoaling at the Paleocene/Eocene Thermal Maximum on Shatsky Rise, northwest Pacific. In: Bralower, T.J., et al. (Eds.), Proc. ODP, Sci Results, 198 (2006), pp. 1-36

R.M. Corfield, J.E. Cartlidge, I. Premoli-Silva, R.A. HousleyOxygen and carbon isotope stratigraphy of the Palaeogene and Cretaceous limestones on the Bottaccione Gorge and the Contessa Highway sections, Umbria, Italy Terra Nova, 3 (1991), pp. 414-422

B.H. CorlissMicrohabitats of benthic foraminifera within deep-sea sediments Nature, 314 (1985), pp. 435-438, B.S. Cramer, J.D. Wright, D.V. Kent, M.-P. AubryOrbital climate forcing of δ13C excursions in the late Paleocene–early Eocene (Chrons C24n–C25n) Paleoceanography, 18 (2003), 10.1029/2003PA000909

Dercourt, J., Ricou, L.E., Vrielynck, B., 1993. Atlas Tethys Palaeoenvironmental Maps: Paris, Gauthier Villars, 307 p.

G.R. Dickens, J.R. O'Neil, D.K. Rea, R.M. OwenDissociation of oceanic methane hydrate as a cause of the carbon isotope excursion at the end of the Paleocene Paleoceanography, 10 (1995), pp. 965-971, 10.1029/95PA02087

G.R. Dickens, M.M. Castillo, J.C.G. WalkerA blast of gas in the latest Paleocene: simulating first-order effects of massive dissociation of oceanic methane hydrate Geology, 25 (1997), pp. 259-262

R. EgliCharacterization of individual rock magnetic components by analysis of remanence curves. 3. Bacterial magnetite and natural processes in lakes. Phys Chem. Earth, 29 (2004), pp. 869-884

Egli, R., Chen, A.P., Winklhofer, M., Kodama, K.P., Horng, C.S., 2010. Detection of noninteracting single domain particles using first-order reversal curve diagrams. Geochem. Geophys. Geosyst. 11, Q01Z11. doi:https://doi.org/10.1029/2009GC002916.

Evans, M.E., Heller, F., 2003. Environmental magnetism. Principles and Applications of Enviromagnetics Academic Press, 299 pp.

E. Font, A. Nédélec, B.B. Ellwood, J. Mirão, P.F. SilvaA new sedimentary benchmark for the Deccan Traps volcanism? Geophys. Res. Lett., 38 (2011), Article L24309, 10.1029/2011GL049824

E. Font, S. Fabre, A. Nédélec, T. Adatte, G. Keller, C. Veiga-Pires, J. Ponte, J. Mirão, H. Khozyem, J.E. SpangenbergAtmospheric halogen and acid rains during the main phase of Deccan eruptions: magnetic and mineral evidence G. Keller, A.C. Kerr (Eds.), Volcanism, Impacts, and Mass Extinctions: Causes and Effects, Geol. Soc. Am. Bull. Spec. Paper, vol. 505 (2014), pp. 353-368

F. Frontalini, R. Coccioni, R. Catanzariti, L. Jovane, J. Savian, M. SprovieriThe Eocene Thermal Maximum 3 (K or X) hyperthermal event: reading the environmental perturbations at Gubbio (Italy), M. Menichetti, R. Coccioni, S. Montanari (Eds.), The Stratigraphic Record of Gubbio: Integrated Stratigraphy of the Late CretaceousPaleogene UmbriaMarche Pelagic Basin, Geol. Soc. Am. Bull. Spec. Paper, vol. 524 (2016), pp. 161-175

S. Gardin, S. MonechiPalaeoecological change in middle to low latitude calcareous nannoplankton at the Cretaceous/Tertiary boundary Bull. Soc. Geol. France, 169 (1998), pp. 709-723

S.J. Gibbs, T.J. Bralower, P.R. Bown, J.C. Zachos, L. BybellShelf-open ocean calcareous phytoplankton assemblages across the Paleocene–Eocene Thermal Maximum: implications for global productivity gradients Geology, 34 (2006), pp. 233-236

Hancock, H.J.L., Dickens, G.R., 2005. Carbonate dissolution episodes in Paleocene and Eocene sediment, Shatsky Rise, West-Central Pacific. Proc. ODP, Sci. Res. 198, College Station, TX, 1–58. Haq and Lohmann, 1976

B.U. Haq, G.P. LohmannEarly Cenozoic calcareous nannoplankton biogeography of the Atlantic Ocean: Mar Micropaleontol., 1 (1976), pp. 119-194

W.W. Hay, R.M. DeConto, C.N. Wold, K.M. Wilson, S. Voigt, M. Schulz, A.R. Wold, W.-C. Dullo, A.B. Ronov, A.N. Balukhovsky, E. SödingetAlternative global Cretaceous paleogeography E. Barrera, C. Johnson (Eds.), Evolution of the Cretaceous Ocean-Climate System, Geol. Soc. Am. Bull. Spec. Paper, vol. 332 (1999), pp. 1-47, 10.1130/0-8137-2332-9.1

J.C. Herguera, W.H. BergerPaleoproductivity from benthic foraminifera abundance: glacial to postglacial change in the west-equatorial Pacific Geology, 19 (1991), pp. 1173-1176

Heslop, D., Roberts, A.P., 2012. Estimation of significance levels and confidence intervals for first-order reversal curve distributions. Geochem. Geophys. Geosyst. 13, Q12Z40. doi:https://doi.org/10.1029/2012GC004115.

D. Heslop, A.P. Roberts, L. ChangCharacterizing magnetofossils from first-order reversal curve (FORC) central ridge signatures Geochem. Geophys. Geosyst., 15 (2014), pp. 2170-2179, 10.1002/2014GC005291

A.G. Hewaidy, S. Farouk, Y.S. BazeenThe Selandian/Thanetian transition of the Naqb El-Rufuf section Foraminiferal biostratigraphy and sequence stratigraphy implications. J African Earth Scie, Kharga Oasis, Western Desert, Egypt (2019), 10.1016/j.jafrearsci.2018.10.002 (in press)

F.J. Hilgen, K.F. Kuiper, L.J. LourensEvaluation of the astronomical time scale for the Paleocene and earliest Eocene Earth Planet. Sci. Lett., 300 (2010), pp. 139-151

C.J. Hollis, G.R. Dickens, B.D. Field, C.-M. Jones, C.P. StrongThe Paleocene-Eocene transition at Mead Stream, New Zealand: a southern Pacific record of early Cenozoic global change Palaeogeogr. Palaeoclimatol. Palaeoecol., 215 (2005), pp. 313-343

S.J. Hunter, A.M. Haywood, P.J. Valdes, J.E. Francis, M.J. PoundModelling equable climates of the Late Cretaceous: can new boundary conditions resolve data-model discrepancies? Palaeogeogr. Palaeoclimatol. Palaeoecol., 392 (2013), pp. 41-51, 10.1016/j. palaeo.2013.08.009

E.G. Hyland, N.D. Sheldon, J.M. CottonTerrestrial evidence for a two stage mid Paleocene biotic event Palaeogeogr. Palaeoclimatol. Palaeoecol., 417 (2015), pp. 371-378

M.J. Johnsson, R.C. ReynoldsClay mineralogy of shale-limestone rhythmites in the Scaglia Rossa (Turonian-Eocene), Italian Apennines J. Sediment. Petrol., 56 (1986), pp. 501-509

L. Jovane, F. Florindo, J. Dinares-TurellEnvironmental magnetic record of paleoclimate change from the Eocene-Oligocene stratotype section, Massignano Italy. Geophys. Res. Lett., 31 (2004), Article L15601, 10.1029/2004GL020554

L. Jovane, R. Coccioni, A. Marsili, G. ActonThe late Eocene greenhouse-icehouse transition: observations from the Massignano global stratotype section and point (GSSP). In: Koeberl, C. & Montanari, A. (eds) The Late Eocene Earth – Hothouse, Icehouse, and Impacts Geological Society of America, Boulder, CO, Special Papers, 452 (2009), pp. 149-168

L. Jovane, M. Sprovieri, R. Coccioni, F. Florindo, A. Marsili, J. LaskarAstronomical calibration of the middle Eocene Contessa Highway section (Gubbio, Italy) Earth Planet. Sci. Lett., 298 (2010), pp. 77-88
L. Jovane, F. Florindo, D.A. Bazylinski, U. LinsPrismatic magnetite magnetosomes from cultivated Magnetovibrio blakemorei strain MV-1: a magnetic fingerprint in marine sediments? Environ. Microbiol. Rep., 4 (2012), pp. 664-668, 10.1111/1758-2229
Kaminski, M.A., Gradstein, F.M., 2005. An atlas of Paleogene cosmopolitan deep-water agglutinated Foraminifera. Grzybowski Foundation, Spec. Publication 10.
N. Karoui-Yaakoub, M. Said Mtimet, M. Hédi Negra, C. Grira, W. GusemiThe registration of the Mid-Paleocene biotic event (MPBE) in Tunisia Paleontology J., 760436 (2014)
S.D. Killops, C.J. Hollis, H.E.G. Morgans, R. Sutherland, B.D. Field, D.A. LeckiePaleoceanographic significance of Late Paleocene dysaerobia at the shelf/slope break around New Zealand Palaeogeogr. Palaeoclimatol. Palaeoecol., 156 (2000), pp. 51-70
L. Kocsis, E. Gheerbrant, M. Mouflih, H. Cappetta, J. Yans, M. AmaghzazComprehensive stable isotope investigation of marine biogenic apatite from the late Cretaceous–early Eocene phosphate series of Morocco Palaeogeogr. Palaeoclimatol. Palaeoecol., 394 (2014), pp. 74-88
Kruiver, P.P., Passier, H.F., 2001. Coercivity analysis of magnetic phases in sapropel S1 related to variations in redox conditions, including an investigation of the S-ratio. Geochem. Geophys. Geosyst. 2 (2001GC000181).
P.P. Kruiver, M.J. Dekkers, D. HeslopQuantification of magnetic coercivity components by the analysis of acquisition curves of isothermal remanent magnetization Earth Planet. Sci. Lett., 189 (2001), pp. 269-276
W. Kuhnt, M.A. KaminskiThe response of benthic foraminifera to the K/T boundary event: a review. In: Jardine, S., De Klasz, I., Debenay, J.P. (Eds.), Geologie de l'Afrique et de l'Atlantique Sud – Compte-rendu des colloques de geologie d'Angiers. Bull. Cent. Rech Exploration-Production Elf Aquitaine, Memoir, 16 (1996), pp. 433-442
J.C. Larrasoaña, A.P. Roberts, L. Chang, S.A. Schellenberg, J.D. Fitz Gerald, R.D. Norris, J.C. ZachosMagnetotactic bacterial response to Antarctic dust supply during the Paleocene–Eocene thermal maximum Earth Planet. Sci. Lett., 333–334 (2012), pp. 122-133
L. Leon-Rodriguez, G.R. DickensConstraints on ocean acidification associated with rapid and massive carbon injections: the early Paleogene record at Ocean Drilling Program Site 1215, equatorial Pacific Ocean Palaeogeogr. Palaeoclimatol. Palaeoecol., 298 (2010), pp. 409-420
F. LirerA new technique for retrieving calcareous microfossils from lithified lime deposits: Micropaleontology 46, 365–369 (2000)
K. Littler, U. Röhl, T. Westerhold, J.C. ZachosA high-resolution benthic stable-isotope record for the South Atlantic: implications for orbital-scale changes in Late Paleocene–Early Eocene climate and carbon cycling Earth Planet. Sci. Lett., 401 (2014), pp. 18-30
Q. Liu, A.P. Roberts, J.C. Larrasoaña, S.K. Banerjee, Y. Guyodo, L. Tauxe, F. OldfieldEnvironmental magnetism: principles and applications Rev. Geophys., 50 (2012), Article RG4002, 10.1029/2012RG000393
S.Z. Liu, C.L. Deng, J.L. Xiao, J.H. Li, G.A. Paterson, L. Chang, L. Yi, H.F. Qin, Y.X. Pan, R.X. ZhuInsolation driven biomagnetic response to the Holocene Warm Period in semi-arid East Asia Sci. Rep., 5 (2015), p. 8001
J.L. Lourens, A. Sluijs, D. Kroon, J.C. Zachos, E. Thomas, U. Röhl, J. Bowles, I. RaffiAstronomical pacing of late Paleocene to early Eocene global warming events Nature, 435 (2005), pp. 1083-1087
W. Lowrie, W. Alvarez, G. Napoleone, K. Perch-Nielsen, I. Premoli Silva, M. ToumarkinePaleogene magnetic stratigraphy in Umbrian pelagic carbonate rocks: the Contessa sections Gubbio. Geol. Soc. Am. Bull., 93 (1982), pp. 414-432
V. Luciani, L. Giusberti, C. Agnini, J. Backman, E. Fornaciari, D. RioThe Paleocene–Eocene Thermal Maximum as recorded by Tethyan planktonic foraminifera in the Forada section (northern Italy) Mar. Micropaleontol., 64 (2007), pp. 189-214
V. Luciani, L. Giusbert, C. Agnini, E. Fornaciari, D. Rio, D.J.A. Spofforth, H. PälikeEcological and evolutionary response of Tethyan planktonic foraminifera to the middle Eocene climatic optimum (MECO) from the Alano section (NE Italy) Palaeogeogr. Palaeoclimatol. Palaeoecol., 292 (2010), pp. 82-95
B.A. MaherMagnetic properties of some synthetic sub-micron magnetites Geophys. J., 94 (1988), pp. 83-96, E. MartiniStandard Tertiary and Quaternary calcareous nannoplankton zonation A. Farinacci (Ed.), Proceedings of the Second Planktonic Conference, 2, Edizioni Tecnoscienza, Rome (1971)
B.M. Moskowitz, R.B. Frankel, D.A. Bazylinski, H.W. Jannasch, D.R. LovleyA comparison of magnetite particles produced anaerobically by magnetotactic and dissimilatory iron-reducing bacteria Geophys. Res. Lett., 16 (1989), pp. 665-668
M.J. Nicolo, G.R. Dickens, C.J. Hollis, J.C. ZachosMultiple early Eocene hyperthermals: their sedimentary expression on the New Zealand continental margin and in the deep sea Geology, 35 (2007), pp. 699-702

H. Okada, D. BukrySupplementary modification and introduction of code numbers to the low-latitude coccoliths biostratigraphic zonation (Bukry, 1973; 1975) Mar. Micropaleontol., 5 (1980), pp. 321-325
M. Pagani, N. Pedentchouk, M. Huber, A. Sluijs, S. Schouten, H. Brinkhuis, J.S. Sinninghe Damsté, G.R. Dickens, Expedition-ScientistsArctic hydrology during global warming at the Palaeocene–Eocene thermal maximum Nature, 442 (2006), pp. 671-675
H. Pälike, R.D. Norris, J.O. Herrle, P.A. Wilson, H.K. Coxall, C.H. Lear, N.J. Shackleton, A.K. Tripati, B.S. WadeThe heartbeat of the Oligocene climate system Science, 314 (2006), pp. 1894-1898
D. Persico, G. VillaEocene-Oligocene calcareous nannofossils from Maud Rise and Kerguelen Plateau (Antarctica): paleoecological and paleoceanographic implications Mar. Micropaleontol., 52 (2004), pp. 153-179
Petrizzo, M.R., 2005. An early late Paleocene event on Shatsky Rise, northwest Pacific Ocean (ODP Leg 198): evidence from planktonic foraminiferal assemblage. Proc. ODP, Sci. Res. 198, College Station, TX, 1–29.
C.R. Pike, A.P. Roberts, K.L. VerosubCharacterizing interactions in fine magnetic particle systems using first order reversal curves J. Appl. Phys., 85 (1999), pp. 6660-6667
V. Pujalte, X. Orue-Etxebarria, E. Apellaniz, F. Caballero, S. Monechi, S. Ortiz, B. SchmitzA prospective Early Late Paleocene event (ELPE) from the expanded Río Gor hemipelagic section (Betic Cordillera, southern Spain): foraminifera, nannofossil and isotopic data Rend. Online Soc. Geol. It., 31 (2014), pp. 181-182
V. Pujalte, E. Apellaniz, F. Santamaria, S. Monechi, S. Ortiz, X. Orue-Etxebarria, F. Caballero, F. Rodríguez-Tovar, B. SchmitzIntegrative stratigraphy and climatic events of a new lower Paleogene reference section from the Betic Cordillera: Río Gor, Granada province SE Spain. Spanish J. Palaeon., 32 (2016), pp. 185-206
I. Raffi, J. Backman, J.C. Zachos, A. SluijsThe response of calcareous nannofossil assemblages to the Paleocene Eocene Thermal Maximum at the Walvis Ridge in the South Atlantic Mar. Micropaleontol., 70 (2009), pp. 201-212
Rio, D., Fornaciari, E., and Raffi, I., 1990. Late Oligocene through early Pleistocene calcareous nannofossils from western equatorial Indian Ocean (Leg 115). Proc. ODP, Sci. Res. 115, College Station, TX, 175–235.
A.P. Roberts, C.R. Pike, K.L. VerosubFORC diagrams: a new tool for characterizing the magnetic properties of natural samples J. Geophys. Res., 105 (2000), pp. 28461-28475
A.P. Roberts, F. Florindo, G. Villa, L. Chang, L. Jovane, S.M. Bohaty, J.C. Larrasoaña, D. Heslop, J.D. Fitz GeraldMagnetotactic bacterial abundance in pelagic marine environments is limited by organic carbon flux and availability of dissolved iron Earth Planet. Sci. Lett., 310 (2011), pp. 441-452
A.P. Roberts, L. Chang, D. Heslop, F. Florindo, J.C. LarrasoañaSearching for single domain magnetite in the “pseudo-single-domain” sedimentary haystack: implications of biogenic magnetite preservation for sediment magnetism and relative paleointensity determinations J. Geophys. Res., 117 (2012), Article B08104
A.P. Roberts, F. Florindo, L. Chang, D. Heslop, L. Jovane, J.C. LarrasoañaMagnetic properties of pelagic marine carbonates Earth-Sci. Rev., 127 (2013), pp. 111-139
D.J. Robertson, D.E. FranceDiscrimination of remanence-carrying minerals in mixtures, using isothermal remanent magnetisation acquisition curves Phys. Earth Planet. Inter., 82 (1994), pp. 223-234
D. Rodelli, L. Jovane, A. Roberts, J. Cypriano, F. Abreu, U. LinsFingerprints of partial oxidation of biogenic magnetite from cultivated and natural marine magnetotactic bacteria using synchrotron radiation Env. Microbio. Reports, 10 (2018), pp. 337-343, 10.1111/1758-2229.12644
W.M. Roggenthen, G. NapoleoneThe Gubbio section, Upper Cretaceous-Paleocene magnetic stratigraphy Geol. Soc. Am. Bull., 88 (1977), pp. 378-382
U. Röhl, T. Westerhold, T.J. Bralower, M.-R. Petrizzo, J.C. ZachosAn early late Paleocene global dissolution event and new constraints for an astronomically-tuned early Paleogene time scale, abstract 8th International Conference on Paleoceanography, France, Biarritz (2004)
G. Rosenbaum, G.S. Lister, C. DuboisReconstruction of the tectonic evolution of the western Mediterranean since the Oligocene J. Virtual Explorer., 8 (2002), pp. 107-130, 10.3809/jvirtex.2002.00053
P.H. Roth, H. ThierssteinCalcareous nannoplankton: leg 14 of the Deep Sea Drilling Project D.E. Hayes, et al. (Eds.), Init. Rep, DSDP, vol. 14, U.S. Government Printing Office, Washington, D.C. (1972), pp. 421-485
J.F. Savian, L. Jovane, F. Frontalini, R.I.F. Trindade, R. Coccioni, S.M. Bohaty, P.A. Wilson, F. Florindo, A.P. Roberts, R. Catanzariti, F. IacovielloEnhanced primary productivity and magnetotactic bacterial production in response to middle Eocene warming in the Neo-Tethys Ocean Palaeogeogr. Palaeoclimatol. Palaeoecol., 414 (2014), pp. 32-45
J.F. Savian, L. Jovane, M. Giorgioni, F. Iacoviello, D. Rodelli, A.P. Roberts, L. Chang, F. Florindo, M. SprovieriEnvironmental magnetic implications of magnetofossil occurrence during the Middle Eocene Climatic Optimum (MECO) in pelagic sediments from the equatorial Indian Ocean Palaeogeogr. Palaeoclimatol. Palaeoecol., 441 (2016), pp. 212-222, 10.1016/j.palaeo.2015.06.029

B. Schmitz, V. Pujalte, E. Molina, et al.The global stratotype sections and points for the bases of the Selandian (Middle Paleocene) and Thanetian (Upper Paleocene) stages at Zumaia, Spain Episodes, 34 (2011), pp. 220-243

C.J. Schroeder, D.B. Scott, F.S. MedioliCan smaller foraminifera be ignored in paleoenvironmental analyses? J. Foraminifer. Res., 17 (1987), pp. 101-105

Sinnesael, M., De Vleeschouwer, D., Coccioni, R., Claeys, P., Frontalini, F., Jovane, L., Savian, J.F., Montanari, A., 2016. High-resolution multiproxy cyclostratigraphic analysis of environmental and climatic events across the Cretaceous-Paleogene boundary in the classic pelagic succession of Gubbio. In: Menichetti, M., Coccioni, R., and Montanari, S., (Eds.), The Stratigraphic Record of Gubbio: Integrated Stratigraphy of the Late CretaceousPaleogene UmbriaMarche Pelagic Basin. Geol. Soc. Am. Bull. Spec. Paper 524, 115–137. doi:https://doi.org/10.1130/2016.2524(09).

A. Sluijs, H. Brinkhuis, S. Schouten, J.C. Zachos, C.M. John, S. Bohaty, J.S. Sinninghe Damsté, E.M. CrouchEnvironmental precursors to light carbon input at the Paleocene/Eocene boundary Nature, 450 (2007), pp. 1218-1221, 10.1038/nature06400

C. Spötl, T.W. VennemannContinuous-flow isotope ratio mass spectrometric analysis of carbonate mineral Rapid Commun. Mass Spectrom., 17 (2003), pp. 1004-1006

R. Thompson, F. OldfieldEnvironmental Magnetism Allen and Unwin, Winchester, Mass. (1986), 10.1007/978-94-0118036-8. 227 pp

F. Tremolada, T.J. BralowerNannofossil assemblage fluctuations during the Paleocene–Eocene Thermal Maximum at Sites 213 (Indian Ocean) and 401 (North Atlantic Ocean): palaeoceanographic implications Mar. Micropaleontol., 52 (2004), pp. 107-116

A. Turtù, V. Lauretano, R. Catanzariti, F.J. Hilgen, S. Galeotti, L. Lanci, M. Moretti, L.J. LourensIntegrated stratigraphy of the Smirra Core (Umbria-Marche Basin, Apennines, Italy): a new early Paleogene reference section and implications for the geologic time scale Palaeogeogr. Palaeoclimatol. Palaeoecol., 487 (2017), pp. 158-174

G.R. Upchurch, B.L. Otto-Bliesner, C.R. ScoteseTerrestrial vegetation and its effects on climate during the latest Cretaceous E. Barrera, C. Johnson (Eds.), Evolution of the Cretaceous Ocean-Climate System, Geol. Soc. Am. Bull. Spec. Paper, vol. 332 (1999), pp. 407-426, 10.1130/0-8137-2332-9.407

K.L. Verosub, A.P. RobertsEnvironmental magnetism: past, present, and future J. Geophys. Res., 100 (1995), pp. 2175-2192, 10.1029/94JB02713

B.S. Wade, P.N. Pearson, W.A. Berggren, H. PälikeReview and revision of Cenozoic tropical planktonic foraminiferal biostratigraphy and calibration to the geomagnetic polarity and astronomical time scale: Earth-Scie Rev., 104 (2011), pp. 111-142, 10.1016/j.earscirev.2010.09.003

T. Westerhold, U. Röhl, I. Raffi, E. Fornaciari, S. Monechi, V. Reale, J. Bowles, H.F. EvansAstronomical calibration of the Paleocene time Palaeogeogr. Palaeoclimatol. Palaeoecol., 257 (2008), pp. 377-403

T. Westerhold, U. Röhl, B. Donner, H.K. McCarren, J.C. ZachosA complete high-resolution Paleocene benthic stable isotope record for the central Pacific (ODP Site 1209) Paleoceanography, 26 (2011), Article PA2216, 10.1029/2010PA002092

T. YamazakiPaleoposition of the Intertropical Convergence Zone in the eastern Pacific inferred fromglacial–interglacial changes in terrigenous and biogenicmagnetic mineral fractions Geology, 40 (2012), pp. 151-154, 10.1130/G32646.1

T. Yamazaki, K. HoriuchiPrecessional control on ocean productivity in the Western Pacific Warm Pool for the last 400 kyr: insight from biogenic magnetite Geochem. Geophys. Geosyst., 17 (2016), pp. 4399-4412, 10.1002/2016GC006446

T. Yamazaki, M. IkeharaOrigin of magnetic mineral concentration variation in the Southern Ocean Paleoceanography, 27 (2012), Article PA2206, 10.1029/2011PA002271

J.C. Zachos, M.W. Wara, S. Bohaty, M.L. Delaney, M.R. Petrizzo, A. Brill, T.J. Bralower, I. Premoli-SilvaA transient rise in tropical sea surface temperature during the Paleocene–Eocene thermal maximum Science, 302 (2003), pp. 1551-1554

Zachos, J.C., Kroon, D., et al., 2004. Early Cenozoic extreme climates: the Walvis Ridge transect: Proc. ODP, Leg 208: http://www-odp.tamu.edu/publications/208-IR/208ir.htm.

J.C. Zachos, U. Röhl, S.A. Schellenberg, A. Sluijs, D.A. Hodell, D.C. Kelly, E. Thomas, M. Nicolo, I. Raffi, L.J. Lourens, H. McCarren, D. KroonRapid acidification of the ocean during the Paleocene-Eocene Thermal Maximum Science, 308 (2005), pp. 1611-1615

Fig. 1. Paleogeographic reconstruction at 60 Ma and location of the Shatsky Rise (ODP Leg 198, Sites 1209, 1210, 1211, 1212), Walvis Ridge (ODP Leg 208, Sites 1262, 1266, 1267), Maud Rise (ODP Leg 113, Sites 689, 690), Black Nose (ODP Leg 171, Site 1051) and Zumaia, Ibaeta, Rio Gor, Contessa Road, Tejerouine, Naqb El-Rufuf, Ouled Abdoun and Mead Stream on-land sections as well as Cerro Bayo as terrestrial record. Reconstruction made using the web-based software at http://www.odsn.de/odsn/services/paleomap/paleomap.html.

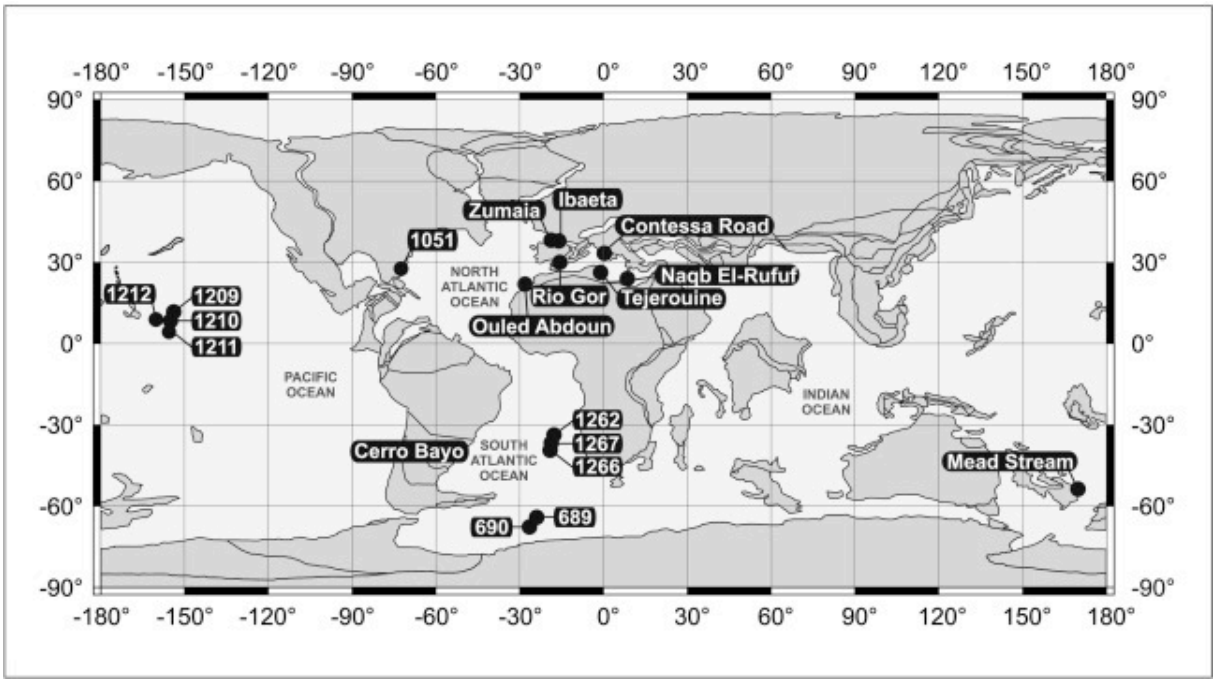

Fig. 2. Changes in CaCO3 content, δ13C and δ18O of bulk sediments, magnetic susceptibility (χ), rock magnetic properties (isothermal remanent magnetization, IRM; anhysteretic remanent magnetization, ARM; ARM/IRM ratio; hard isothermal remanent magnetization, HIRM300; S-ratio300), and coarse fraction across the 8 m-thick studied segment (~800 kyr) spanning the Selandian–Thanetian transition at Contessa Road. Biostratigraphy is based on the planktonic foraminiferal Zones of Wade et al. (2011) and calcareous nannoplankton Zones of Martini (1971) and Okada and Bukry (1980). Magnetostratigraphy is from Coccioni et al. (2016). The interval 1 represents the Pre-STTE event, interval 2 the STTE event, interval 3 the equivalent of the ELPE event and interval 4 the Post-STTE event.

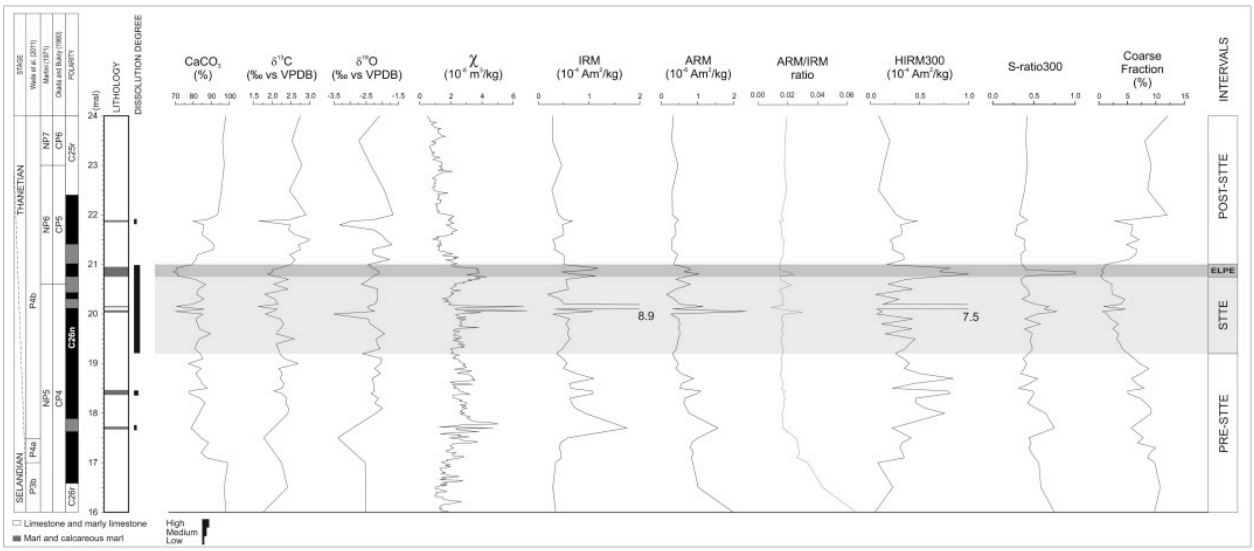

Fig. 3. (a) IRM acquisition data with cumulative log-Gaussian function (Robertson and France, 1994; Kruiver et al., 2001) for three representative samples from Contessa Road. Component 1 is interpreted to be detrital magnetite, components 2 and 3 are interpreted as biogenic soft (BS) and biogenic hard (BH), respectively, and marks a dominant contribution. The highest coercivity components 4 and 5 suggest the presence of hematite and/or goethite. (b) Bi-plot showing the calculated components treated by the cumulative log-Gaussian function (Kruiver et al., 2001). (c) Coercivity component contribution vs. stratigraphic position. The stratigraphic position of the samples is shown in Fig. 2. (For interpretation of the references to color in this figure, the reader is referred to the web version of this article.)

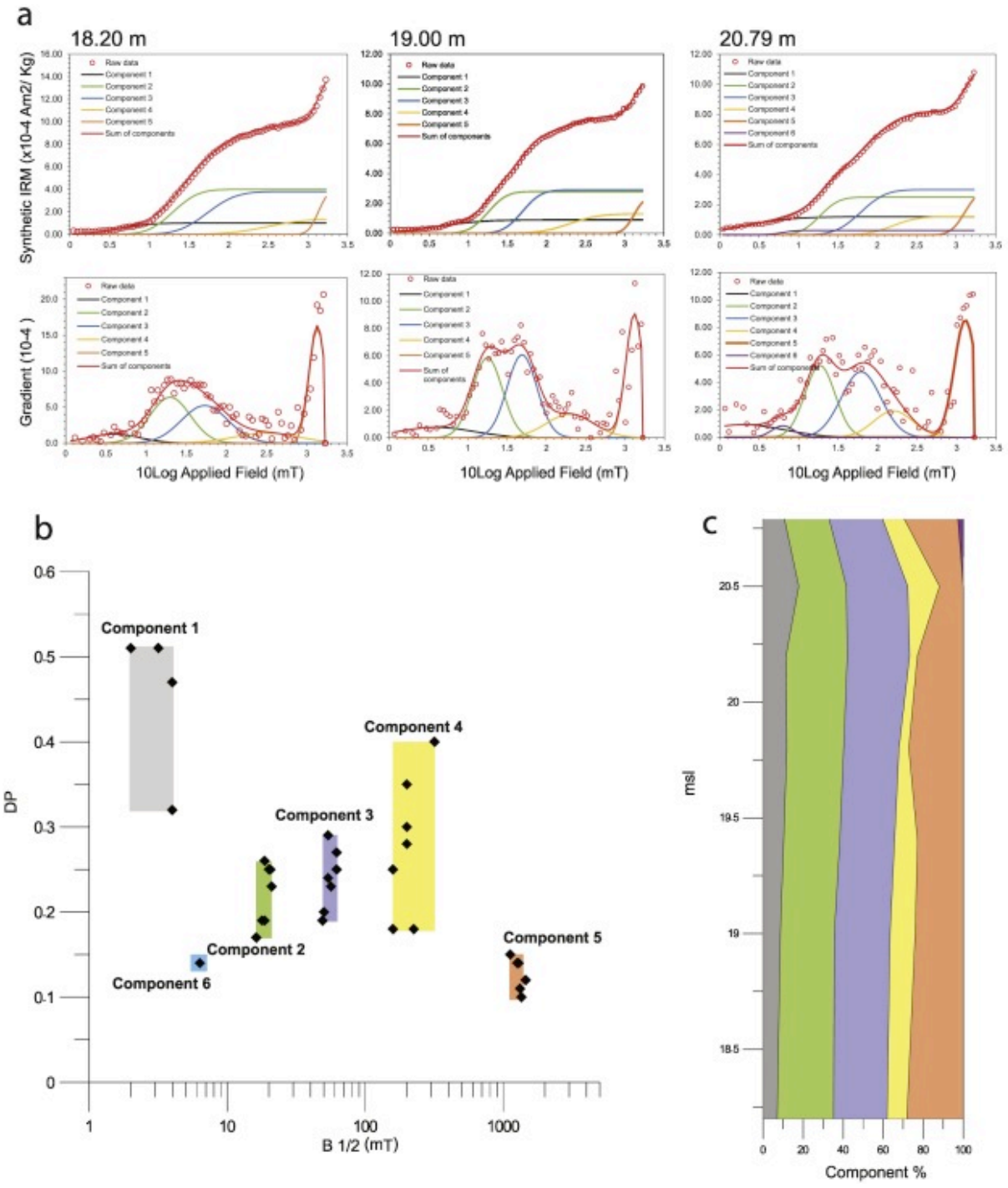

Fig. 4. FORC diagrams (left), coercivity profiles along Bu = 0 (middle), and vertical interaction field profiles through the peak of the FORC distribution (right) for four representative samples that comprehends the Post-STTE (a), ELPE (b), STTE (c), and Pre-STTE (d). The data were processed using the algorithm of Heslop and Roberts (2012). The results shown narrow “central ridge” that indicates non-interacting SD magnetic behaviour (Roberts et al., 2000; Egli et al., 2010) and maxima for the coercivity spectra at about 30 mT during the STTE and ELPE events. The smoothing factor (SF) is 5 for all FORC diagrams (Roberts et al., 2000).

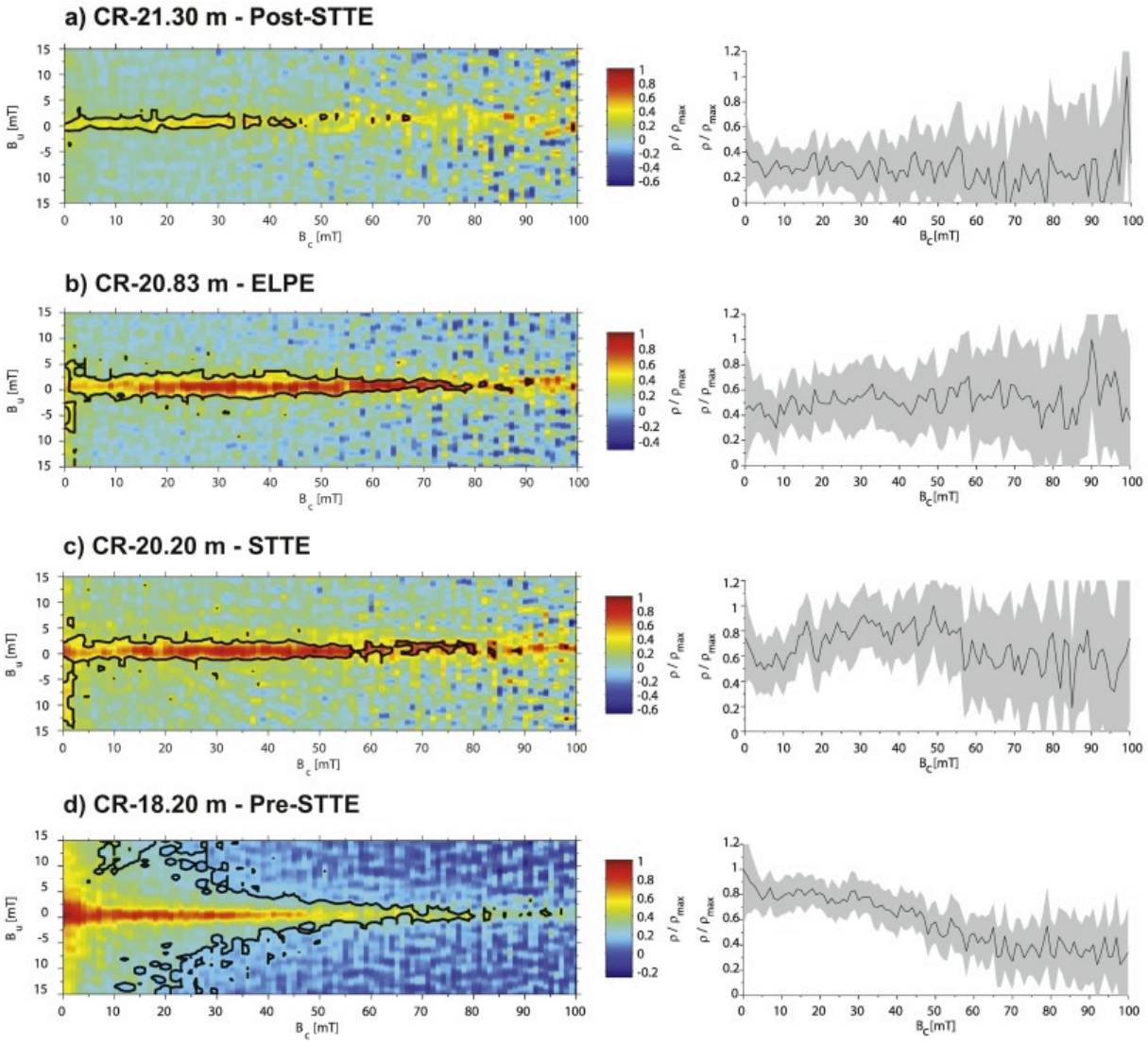

Fig. 5. Changes in selected calcareous nannofossil genera, species, and ecological groups across the 18–22 m segment at Contessa Road. Magneto-bio-chronostratigraphy as in Fig. 2.

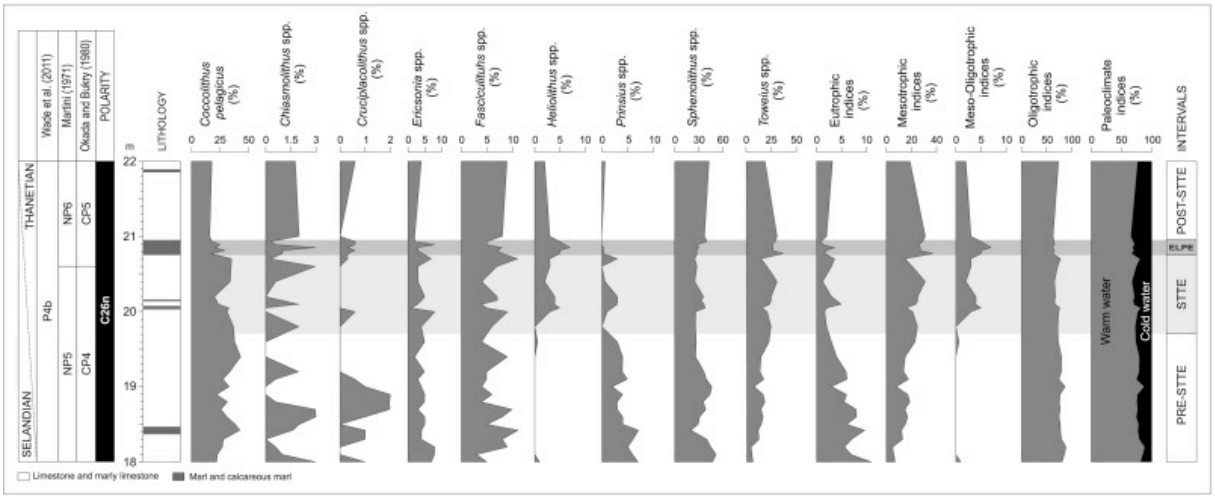

Fig. 6. Changes in selected planktonic foraminiferal genera, species, and morphospecies and fragmentation index across the 18–22 m segment at Contessa Road. Magneto-bio-chronostratigraphy as in Fig. 2.

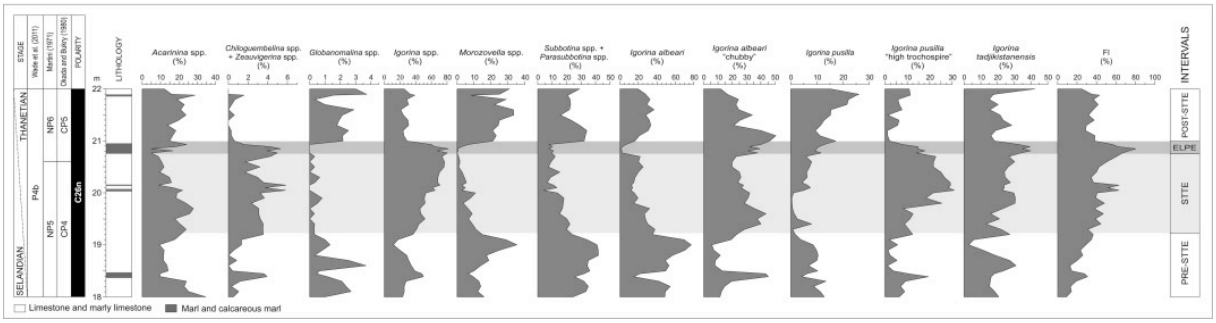

Fig. 7. Changes in selected benthic foraminiferal parameters [P/(P + B) ratio, foraminiferal density (FD), agglutinans vs. calcareous ratio, and infauna vs. epifauna ratio] and the relative abundance of Spiroplectammina spp. across the across the 18–22 segment at Contessa Road. Magneto-bio-chronostratigraphy as in Fig. 2.

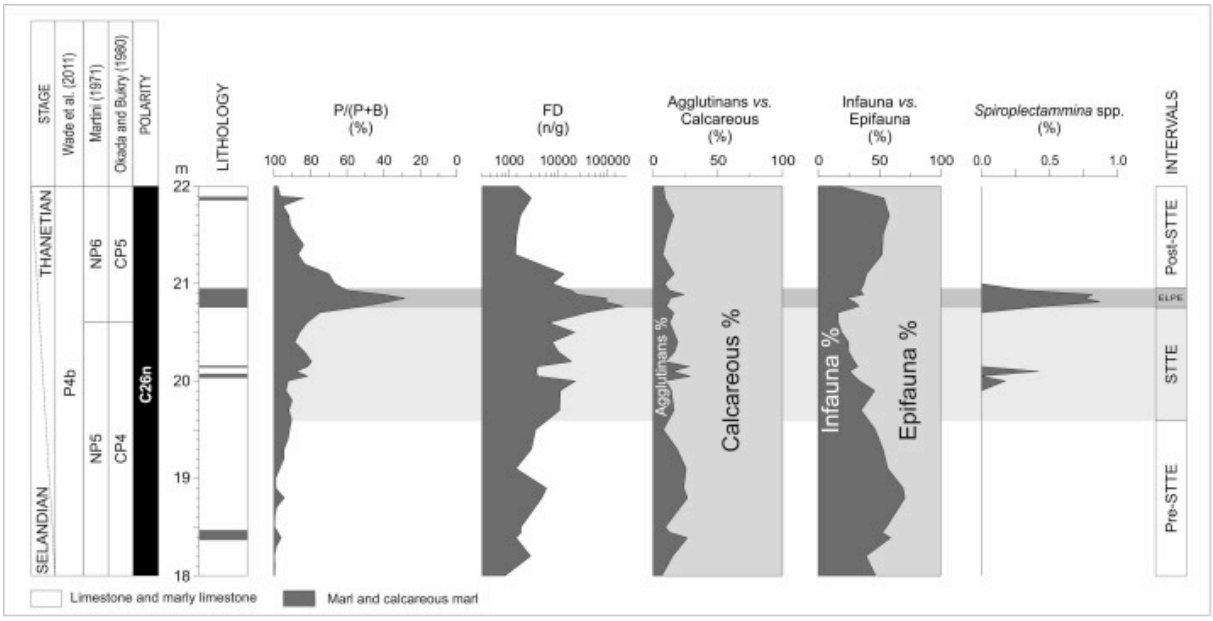

Fig. 8. Summary of the main dissolution proxies, main biotic events and changes, and inferred paleoenvironmental conditions across the 8 m-thick studied segment spanning the Selandian–Thanetian transition at Contessa Road. Coarse fraction, fragmentation index, and P/(P + B) ratio have been smoothed by an adjacent moving average with a five-point window. Magneto-bio-chronostratigraphy as in Fig. 2. The light grey shaded area highlights the Selandian–Thanetian transition event (STTE) event and the dark grey shaded area marks the early late Paleocene hyperthermal event (ELPE) equivalent. On the basis of the biotic and abiotic changes, the studied segment can be subdivided into five discrete intervals, which have a different duration according to the available magnetostratigraphy at Contessa Road.

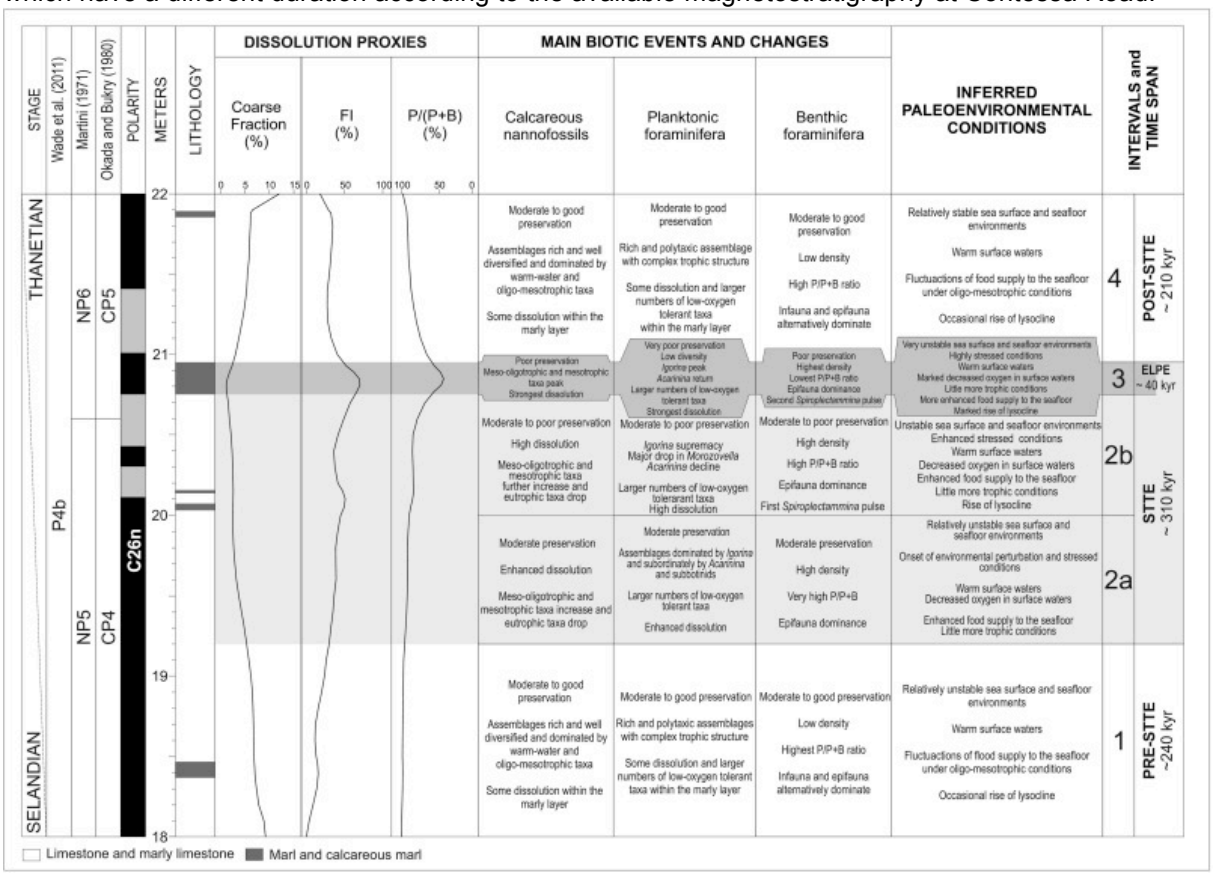

Table 1. Parameters associated with components identified from IRM analysis of seven representative samples from STTE-ELPE of the Contessa Road section.

Sample depth (msl)	Component 1 SIRM (Am^2/kg)	Component 2 SIRM (Am^2/kg)	Component 3 SIRM (Am^2/kg)	Component 4 SIRM (Am^2/kg)	Component 5 SIRM (Am^2/kg)	Component 6 SIRM (Am^2/kg)	Component 1 Contribution (%)	Component 2 Contribution (%)	Component 3 Contribution (%)	Component 4 Contribution (%)	Component 5 Contribution (%)	Component 6 Contribution (%)
18.20	1.00E+00	4.00E+00	3.80E+00	1.40E+00	4.00E+00	–	7	28	27	10	28	–
19.00	9.00E–01	2.80E+00	2.90E+00	1.30E+00	2.50E+00	–	9	27	28	13	24	–
19.40	9.00E–01	2.45E+00	2.40E+00	1.00E+00	2.00E+00	–	10	28	27	11	23	–
19.80	1.00E+00	2.40E+00	2.34E+00	4.10E–01	2.30E+00	–	12	28	28	5	27	–
20.20	9.00E–01	2.40E+00	2.45E+00	3.00E–01	1.80E+00	–	11	31	31	4	23	–
20.50	9.00E–01	1.20E+00	1.55E+00	8.00E–01	6.00E–01	–	18	24	31	16	12	–
20.79	1.20E+00	2.50E+00	3.00E+00	1.21E+00	3.00E+00	3.00E–01	11	22	27	11	27	3

Sample depth (m	Component 1 $B_{1/2}$ (mT	Component 2 $B_{1/2}$ (mT	Component 3 $B_{1/2}$ (mT	Component 4 $B_{1/2}$ (mT	Component 5 $B_{1/2}$ (mT	Component 6 $B_{1/2}$ (mT	Componen Contributi (%)	Componen Contributi (%)	Componen Contributi (%)	Componen Contributi (%)	Componen Contributi (%)	Componen Contributi (%)
18.20	4.0	20.0	53.7	316.2	1349.0	–	7	28	27	10	28	–
19.00	4.0	17.8	49.0	199.5	1318.3	–	9	27	28	13	24	–
19.40	4.0	20.9	53.7	199.5	1349.0	–	10	28	27	11	23	–
19.80	3.2	20.4	61.7	199.5	1445.4	–	12	28	28	5	27	–
20.20	2.0	18.6	56.2	158.5	1122.0	–	11	31	31	4	23	–
20.50	2.0	16.2	50.1	223.9	1258.9	–	18	24	31	16	12	–
20.79	2.0	18.6	61.7	158.5	1288.2	6.3	11	22	27	11	27	3

Sample depth (n	Component 1 DP mT)	Component 2 (l DP mT)	Component 3 (l DP mT)	Component 4 (l DP mT)	Component 5 (l DP mT)	Component 6 (l DP mT)	Componen Contributi (%)	Componen Contributi (%)	Componen Contributi (%)	Componen Contributi (%)	Componen Contributi (%)	Componen Contributi (%)
18.20	0.32	0.25	0.29	0.40	0.10	–	7	28	27	10	28	–
19.00	0.47	0.19	0.19	0.30	0.11	–	9	27	28	13	24	–
19.40	0.47	0.23	0.24	0.35	0.10	–	10	28	27	11	23	–
19.80	0.51	0.25	0.27	0.28	0.12	–	12	28	28	5	27	–
20.20	0.51	0.26	0.23	0.18	0.15	–	11	31	31	4	23	–
20.50	0.51	0.17	0.20	0.18	0.14	–	18	24	31	16	12	–
20.79	0.51	0.19	0.25	0.25	0.14	0.14	11	22	27	11	27	3

IRM data treated by the cumulative log-Gaussian function (Kruiver et al., 2001).